

Gauge Symmetry in Quantum Simulation

Masanori Hanada^{a,*}, Shunji Matsuura^b, Andreas Schäfer^c, and Jinzhao Sun^{d†}

^a*School of Mathematical Sciences, Queen Mary University of London
Mile End Road, London, E1 4NS, United Kingdom*

^a*qBraid Co., Harper Court 5235, Chicago, IL 60615, United States*

^b*Interdisciplinary Theoretical & Mathematical Science Program (iTHEMS), RIKEN
Wako, Saitama 351-0198, Japan*

^b*Department of Electrical and Computer Engineering
University of British Columbia, Vancouver, BC V6T 1Z4, Canada*

^c*Institute of Theoretical Physics, University of Regensburg
Universitätsstrasse 31, D-93053 Regensburg, Germany*

^c*Department of Physics, National Taiwan University, Taipei, Taiwan 106*

^d*School of Physical and Chemical Sciences, Queen Mary University of London
Mile End Road, London, E1 4NS, United Kingdom*

Quantum simulation of non-Abelian gauge theories requires careful handling of gauge redundancy. We address this challenge by presenting universal principles for treating gauge symmetry that apply to any quantum simulation approach, clarifying that physical states need not be represented solely by gauge singlets. Both singlet and non-singlet representations are valid, with distinct practical trade-offs, which we elucidate using analogies to BRST quantization. We demonstrate these principles within a complete quantum simulation framework based on the orbifold lattice, which enables explicit and efficient circuit constructions relevant to real-world QCD. For singlet-based approaches, we introduce a Haar-averaging projection implemented via linear combinations of unitaries, and analyze its cost and truncation errors. Beyond the singlet-approach, we show how non-singlet approaches can yield gauge-invariant observables through wave packets and string excitations. This non-singlet approach is proven to be both universal and efficient. Working in temporal gauge, we provide explicit mappings of lattice Yang–Mills dynamics to Pauli-string Hamiltonians suitable for Trotterization. Classical simulations of small systems validate convergence criteria and quantify truncation and Trotter errors, showing concrete resource estimates and scalable circuit recipes for $SU(N)$ gauge theories. Our framework provides both conceptual clarity and practical tools toward quantum advantage in simulating non-Abelian gauge theories.

I. INTRODUCTION

Gauge symmetry is a fundamental feature of many physical theories, including electromagnetism, Yang–Mills theory [1–3], and Quantum Chromodynamics (QCD) [4–7], and more broadly, the standard model of particle physics [8–12]. They also lie at the core of the most concrete approaches to quantum gravity through dualities between supersymmetric Yang–Mills theories and string/M-theory [13]. Less widely appreciated is that permutation symmetry in systems of identical bosons [14, 15] functions as a gauge symmetry with physical consequences — the Bose–Einstein condensation [16, 17]. Any faithful quantum simulation of such systems must confront the role of gauge symmetry at a fundamental level. While it is often stated that physical states must be gauge-invariant [18], this statement obscures an important distinction between physical equivalence and representation: gauge symmetry — or rather, gauge redundancy — identifies physically equivalent configurations, but does not uniquely prescribe how those configurations should be represented in a quantum simulation. As a result, different representations of physical

states — gauge singlet and non-singlet alike — can be equally valid, provided they encode the same equivalence class and reproduce gauge-invariant observables.

Recent work established quantum circuit constructions for Yang–Mills theory using extended Hilbert space and non-compact variables [19–22], in such a way that the generalization to QCD is straightforward [23]. However, crucial questions regarding the treatment of gauge redundancy remained: how to implement gauge-singlet constraints (when necessary), and when to use singlet or non-singlet formulations. Furthermore, it was not very clear how to validate convergence criteria concerning the truncation of the infinite-dimensional Hilbert space associated with bosons. We address these by: (1) introducing the first singlet projection protocol for $SU(N)$ gauge theory via Haar averaging realized through Linear Combination of Unitaries, (2) establishing universal principles for gauge symmetry treatment applicable to any quantum simulation approach, and (3) providing systematic numerical validation and complete resource estimates. Our framework completes the quantum simulation toolkit for non-Abelian gauge theories, providing both conceptual clarity and practical implementation protocols with validated scalings.

Yang–Mills theory is a natural generalization of electromagnetism, which is a gauge theory with the $U(1)$ gauge group, to the $SU(N)$ gauge group. As in electro-

* m.hanada@qmul.ac.uk

† jinzhao.sun@qmul.ac.uk

magnetism, gauge symmetry plays a crucial role in the quantization of the relativistic theory without negative-norm modes in the Hilbert space. To see this, imagine creation operators \hat{a}_μ^\dagger corresponding to the $U(1)$ gauge field A_μ , where $\mu = 0, 1, 2, 3, 4 = t, x, y, z$, act on the Lorentz-invariant vacuum $|\text{VAC}\rangle$. Then, the natural inner product that is consistent with the Lorentz symmetry is $\langle \text{VAC} | \hat{a}_\mu \hat{a}_\nu^\dagger | \text{VAC} \rangle = \eta_{\mu\nu}$, where $\eta_{\mu\nu} = (-1)^{\delta_{\mu,0}} \delta_{\mu\nu}$. This seems to be a problem because $\hat{a}_\mu^\dagger |\text{VAC}\rangle$ has a negative norm (specifically, the norm is -1 for $\mu = 0$), which could conflict with the probability interpretation of quantum mechanics. Gauge symmetry cures this problem because only the transverse modes are physical, and negative-norm modes decouple from physical processes.

The temporal gauge ($A_t = 0$ gauge; see Supplementary Material S2) is convenient for quantum simulations, because the negative-norm modes are absent; if the Hilbert space contains negative-norm states, it is unclear how to map it to qubits. Some caution is required because this gauge condition does not remove gauge redundancy completely. A common option is to restrict the Hilbert space to be invariant under the residual gauge symmetry; we call such a Hilbert space the gauge-invariant Hilbert space, or the singlet Hilbert space, and denote it by \mathcal{H}_{inv} . This is a subspace of the extended Hilbert space \mathcal{H}_{ext} that contains both gauge singlets and non-singlets. This singlet-prescription is, however, not straightforward. If one tries to construct only \mathcal{H}_{inv} on quantum devices, it is difficult to build orthonormal basis, and the operators including the Hamiltonian become complicated. This leads to exponential growth in classical pre-processing cost, and possibly also in the circuit depth, with respect to the number of logical qubits, which destroys any potential quantum advantage [24]. Therefore, we will use \mathcal{H}_{ext} for quantum simulations. Still, \mathcal{H}_{inv} is realized as a subspace of \mathcal{H}_{ext} , and one has the option to use only states in \mathcal{H}_{inv} .

As established in refs. [20–23], the orbifold lattice framework provides explicit quantum circuit construction for $SU(N)$ gauge theories with polynomial resource scaling, both on quantum devices (the number of gates and circuit depth) and on classical computers (pre-processing cost for designing and compiling quantum circuits). Alternative approaches either lack explicit circuits or require exponential classical compilation [24]. Building on this foundation, we now address the issues associated with gauge symmetry. This paper makes two interconnected contributions:

Universal conceptual framework: We clarify how gauge symmetry should be treated in quantum simulations, resolving some misconceptions and providing principles applicable to any approach. (Sec. II)

Complete practical implementation: We provide explicit protocols, circuits, and resource estimates within the orbifold lattice framework, completing recent advances [20–23] by addressing the treatment of gauge symmetry. To the best of our knowledge, this is the only

approach that provides explicit quantum circuits for Yang-Mills theory, enabling scalable simulation toward the continuum limit without exponential classical compilation costs; see ref. [24] for the cost analyses for other approaches. (Sec. III, Sec. IV, Sec. V, and Sec. VI)

The protocols presented here may appear straightforward to quantum algorithm experts — **this simplicity is precisely the achievement**. Through careful physics-based problem design (specifically, temporal gauge quantization, non-compact variables, and the orbifold lattice Hamiltonian), we reduced a seemingly intractable problem to one where textbook quantum algorithms suffice. The difficulty lies not in inventing new algorithms, but in recognizing which physics reformulation enables algorithmic tractability.

Table I summarizes the key capabilities added in this work compared to the prior orbifold lattice framework (dubbed the “Universal framework” [21]) [20–23] and generic gauge-invariant approaches.

Outline of the paper

In this work, we explain how quantum simulations can be conducted respecting gauge symmetry. We will consider both protocols with and without the singlet constraint. In Sec. II, we start with emphasizing a simple fact: using gauge singlets is only one of many ways to represent physical states. We can choose a convenient option depending on the device and the problem in our hands. We provide analogies with a well-known example — the Becchi-Rouet-Stora-Tyutin (BRST) quantization [2, 3, 25] — that provides us with a better intuition for the meaning of “physical states”, and a few examples of non-singlet descriptions to illustrate the important points.

Whether one uses singlets or non-singlets for quantum simulations, it is convenient if one can project arbitrary non-singlet states to the corresponding singlet states. In Sec. III, we provide such a procedure for $SU(N)$ gauge theory for any N and any dimension. The projection naturally adopts a form of Linear Combinations of Unitaries (LCU) [26] or Quantum Singular Value Transformation (QSVT) [27, 28] and thus can be implemented on a quantum computer. To do so, the use of non-compact variables is a key ingredient. This projection makes simulations with singlet states technically straightforward. As simulations with non-singlet states, we consider two options in Sec. IV: non-singlet excitations of a gauge-invariant state and singlet excitations of a wave packet.

Finally, Sec. V provides crucial numerical validation of convergence criteria. Specifically, it presents systematic numerical experiments on simplified S^n models (bosons constrained to n -spheres) that capture the essential physics of the scalar mass terms in the orbifold lattice. These experiments on classical computers quantify

	Gauge-invariant approaches	Orbifold Lattice (prior work)	Orbifold Lattice (this work)
Explicit circuits	\times	✓	✓
Singlet projection	N/A	\times	✓ (expensive)
Non-singlet states	\times	\times (not justified)	✓ (justified)
Compilation cost	Exponential in $N^2 QV$	Polynomial in N , Q , and V	Polynomial in N , Q , and V
Gate count	Unknown	$O(N^4 Q^4 V)$	$O(N^4 Q^4 V)$
Circuit depth	Unknown	$O(N^4 Q^4)$	$O(N^4 Q^4)$
Convergence validation	N/A	\times	✓

TABLE I. Comparison of generic gauge-singlet approaches (methods attempting to work directly in singlet Hilbert space) and the orbifold approach before and after this work. Here, we consider $SU(N)$ theory in $2+1$ or $3+1$ dimensions. Q is the number of qubits per boson, and V is the number of lattice points. Gate counting and circuit depth can change slightly depending on the details of the implementation. ‘‘Convergence validation’’ refers to the validation of the convergence when the Hilbert space truncation is removed ^a. Circuit depth and Gate Depth are for Hamiltonian time evolution. The singlet projection protocol (Sec. III) involves expensive post-selections.

^a Ref. [22] provided the convergence validation without Hilbert space truncation, using the Euclidean path integral.

how truncation error depends on the discretization scale δ_x and mass m , establishing that $\delta_x \lesssim 1/\sqrt{m}$ is required for accurate low-energy physics. As a bonus, this section clarifies how the state $|\mathcal{G}\rangle$ used for the singlet projection protocol introduced in Sec. III can be constructed. These also demonstrate that Trotter step sizes are determined by physical energy scales (like m), not by the ultraviolet cutoff Λ , confirming that high-energy modes don’t spoil the simulation efficiency.

Appendices A and B provide parallel technical reviews of the two main Hamiltonian formulations used throughout the paper. Appendix A covers the Kogut-Susskind formulation, which uses unitary link variables and serves as the standard lattice gauge theory Hamiltonian. It details the operators and their commutation relations, the structure of the Hamiltonian with its electric and magnetic terms, and crucially, how string states (Wilson loops and lines) behave under the Hamiltonian evolution, including their splitting and joining interactions. A technical subsection compares left-acting versus right-acting electric field operators. Appendix B provides analogous material for the orbifold lattice formulation, which uses complex (non-compact) link variables instead of unitary ones. This formulation is central to the paper’s practical implementation because it allows straightforward truncation to finite-dimensional Hilbert spaces and natural expression in terms of Pauli strings, making it far more suitable for quantum circuit design than the Kogut-Susskind approach.

Supplementary Material offers technical details and review materials that make the paper self-contained.

II. EXTENDED HILBERT SPACE, GAUGE-INVARIANT HILBERT SPACE, AND PHYSICAL STATES

A. Hilbert space

We start with discussing what are the ‘Hilbert space’ and ‘physical states’ in gauge theories, and how they should be treated in quantum simulations. These principles apply to any approach, not just the Kogut-Susskind Hamiltonian and the orbifold lattice Hamiltonian, which will be used as concrete examples below. (See Appendices A and B for reviews of these Hamiltonians.)

The Kogut-Susskind Hamiltonian uses unitary link variables $U_{j,\vec{n}}$ as dynamical degrees of freedom, while the orbifold lattice Hamiltonian uses the complex link variables $Z_{j,\vec{n}}$. Here, j and \vec{n} labels spatial directions and lattice points, respectively. $U_{j,\vec{n}}$ and $Z_{j,\vec{n}}$ live on a link connecting points \vec{n} and $\vec{n} + \hat{j}$, where \hat{j} represents a unit vector along the j -direction and not an operator.

The extended Hilbert space corresponds to all possible field configurations that are compatible with the gauge condition $A_t = 0$. It is defined by

$$\mathcal{H}_{\text{ext}} = \otimes_{j,\vec{n}} \mathcal{H}_{j,\vec{n}} = \otimes_{j,\vec{n}} \text{Span} \{ |U\rangle_{j,\vec{n}} \mid U \in \text{SU}(N) \} , \quad (1)$$

where

$$\hat{U}_{j,\vec{n}} |U\rangle_{j,\vec{n}} = U |U\rangle_{j,\vec{n}} \quad U \in \text{SU}(N) , \quad (2)$$

for the Kogut-Susskind formulation and

$$\mathcal{H}_{\text{ext}} = \otimes_{j,\vec{n}} \mathcal{H}_{j,\vec{n}} = \otimes_{j,\vec{n}} \text{Span} \{ |Z\rangle_{j,\vec{n}} \mid Z \in \mathbb{C}^{N \times N} \} , \quad (3)$$

where

$$\hat{Z}_{j,\vec{n}} |Z\rangle_{j,\vec{n}} = Z |Z\rangle_{j,\vec{n}} \quad Z \in \mathbb{C}^{N \times N} , \quad (4)$$

for the orbifold lattice. More precisely, we consider only the Hilbert space of square-integrable wave functions.

The residual gauge transformation (time-independent gauge transformation) by $\Omega \in \mathcal{G} = \prod_{\vec{n}} [\mathrm{SU}(N)]_{\vec{n}}$ is

$$\hat{\Omega} |U\rangle = |U^{(\Omega)}\rangle, \quad U_{j,\vec{n}}^{(\Omega)} \equiv \Omega_{\vec{n}} U_{j,\vec{n}} \Omega_{\vec{n}+\hat{j}}^{-1} \quad (5)$$

and

$$\hat{\Omega} |Z\rangle = |Z^{(\Omega)}\rangle, \quad Z_{j,\vec{n}}^{(\Omega)} \equiv \Omega_{\vec{n}} Z_{j,\vec{n}} \Omega_{\vec{n}+\hat{j}}^{-1}, \quad (6)$$

respectively. States connected to each other by gauge transformation are physically equivalent. In this sense, ‘gauge symmetry’ is gauge *redundancy*. A large fraction of the redundancy has been already removed by taking the $A_t = 0$ gauge. One way to remove the residual redundancy is to use the gauge-invariant Hilbert space:

$$\mathcal{H}_{\mathrm{inv}} = \left\{ |\Phi\rangle \in \mathcal{H}_{\mathrm{ext}} \mid \hat{\Omega} |\Phi\rangle = |\Phi\rangle \text{ for } \forall \Omega \in \mathcal{G} \right\}. \quad (7)$$

Note that, unless the time direction is noncompact or a special boundary condition is taken, the condition $A_t = 0$ cannot be imposed in the literal sense; we can only push A_t to one point in time. As shown in Supplementary Material S2, the integration of this remaining piece of A_t leads to the projection to $\mathcal{H}_{\mathrm{inv}}$,

$$\hat{\mathcal{P}} \equiv \frac{1}{\mathrm{vol}(\mathcal{G})} \int_{g \in \mathcal{G}} dg \hat{g}. \quad (8)$$

Here, the integration is performed over the Haar measure on \mathcal{G} .

B. “Physical states”

There is a parallel between the quantization in $A_t = 0$ gauge and the Lorentz-covariant quantization that uses BRST cohomology [2, 3, 25] (Table II). In our case, setting $A_t = 0$ is analogous to requiring the BRST-closed condition, $\hat{Q}_{\mathrm{BRST}} |\mathrm{physical}\rangle = 0$ — both eliminate the negative norm modes. That is, $\mathcal{H}_{\mathrm{ext}}$ corresponds to $\mathrm{Ker}(\hat{Q}_{\mathrm{BRST}})$. Both $\mathcal{H}_{\mathrm{ext}}$ and $\mathrm{Ker}(\hat{Q}_{\mathrm{BRST}})$ are redundant and physically equivalent states appear multiple times. To remove the redundancy, in our case, we identify the states that differ only by a gauge transformation, while in covariant quantization, states that differ only by BRST-exact states are identified. In more formal terminologies, the true physical Hilbert space without redundancy is the gauge orbit $\mathcal{H}_{\mathrm{ext}}/\mathrm{Ker}(\hat{\mathcal{P}})$ in our case and the BRST cohomology $\mathrm{Ker}(\hat{Q}_{\mathrm{BRST}})/\mathrm{Im}(\hat{Q}_{\mathrm{BRST}})$ for covariant quantization.

It is important to note that the word “physical” is used loosely in a few different ways. In the context of the BRST quantization, that the state is “physical” often means that the norm is not negative, which is guaranteed by requiring $\hat{Q}_{\mathrm{BRST}} |\mathrm{physical}\rangle = 0$. In this weaker

sense, all states in $\mathcal{H}_{\mathrm{ext}}$ are physical. A stronger, and ultimately more useful, meaning of “physical” is the equivalence class obtained after removing redundancies; that is, elements of the BRST cohomology or, in the temporal gauge, elements of $\mathcal{H}_{\mathrm{ext}}/\mathrm{Ker}(\hat{\mathcal{P}})$ obtained by quotienting by gauge orbits. When, in the context of the $A_t = 0$ gauge, people say “physical states are gauge-invariant,” the latter, stronger version is assumed. More precisely, what is meant there is *how to fix residual gauge symmetry*, which is analogous to the ambiguity associated with the BRST-exact states. Two states connected by a residual gauge transformation are equivalent, just as two BRST-closed states are equivalent if the difference is BRST-exact. Therefore, “physical states are gauge-invariant” is a misleading statement. A more precise statement is that *one way to remove the residual gauge redundancy in the $A_t = 0$ gauge is to use the gauge-invariant Hilbert space*.

BRST-exact states are “unphysical” or “redundant”. In this paper, we adopt “redundant” to emphasize that it is associated with the redundancy of $\mathrm{Im}(\hat{Q}_{\mathrm{BRST}})$. In the $A_t = 0$ gauge, $\mathrm{Ker}(\hat{\mathcal{P}})$ is redundant in the same sense. Note, however, there is an important difference: while $\mathrm{Im}(\hat{Q}_{\mathrm{BRST}})$ consists of zero-norm states, $\mathrm{Ker}(\hat{\mathcal{P}})$ consists of positive-norm states. As we will see in Section IV, ‘redundant’ states in $\mathrm{Ker}(\hat{\mathcal{P}})$ can sometimes be perfectly fine for practical computations, in the sense that the same expectation values are obtained.

$A_t = 0$ Gauge Quantization	Covariant Quantization
$A_t = 0$ gauge	BRST-closed condition
$\mathcal{H}_{\mathrm{ext}}$	$\mathrm{Ker}(\hat{Q}_{\mathrm{BRST}})$
$\mathrm{Ker}(\hat{\mathcal{P}})$	$\mathrm{Im}(\hat{Q}_{\mathrm{BRST}})$
Gauge orbits	BRST cohomology
$\mathcal{H}_{\mathrm{ext}}/\mathrm{Ker}(\hat{\mathcal{P}})$	$\mathrm{Ker}(\hat{Q}_{\mathrm{BRST}})/\mathrm{Im}(\hat{Q}_{\mathrm{BRST}})$

TABLE II. Comparison of $A_t = 0$ gauge quantization and Lorentz-covariant BRST quantization.

C. Singlet vs non-singlet

There are many ways to describe a gauge orbit: one can either choose a point on the orbit (non-singlet state) or average over the orbit (singlet state). Below, we will see that both singlet and non-singlet states can describe gauge-invariant physics. Depending on the problems and simulation architectures, different approaches may be appropriate.

Let us consider classical electromagnetism as an example that shows the importance of the use of the extended Hilbert space and non-singlet states. In classical electromagnetism, classical field configurations are not gauge invariant. This is not a problem because physics is determined by field strength (equivalently, electric field

and magnetic field), which is gauge invariant. For explicit computations, it is convenient to fix the gauge and remove the redundancy. Here, let us take the temporal gauge condition $A_t = 0$. This condition does not remove the redundancy completely because time-independent gauge transformations preserve it.

Such classical field configurations correspond to low-energy wave packets in quantum field theory that are localized around the classical value of the field, $A_j^{(\text{cl.})}$. Clearly, the extended Hilbert space \mathcal{H}_{ext} is used. All wave packets related by the gauge transformation are physically equivalent. In principle, one could use the gauge-invariant Hilbert space \mathcal{H}_{inv} using the projector $\hat{\mathcal{P}}$, but no one does that because the same result is obtained anyway.

Let us elaborate on the above. Let $|\Phi\rangle$ be a wave packet around a field configuration $A_j^{(\text{cl.})}$. A gauge transformation by $g \in \mathcal{G}$ maps $|\Phi\rangle$ to $\hat{g}|\Phi\rangle$, which is a wave packet localized around $A_j^{(\text{cl.})} - g^{-1}\partial_j g$ [29]. Any wave packet on the gauge orbit $\{\hat{g}|\Phi\rangle \mid g \in \mathcal{G}\}$ is equally fine for gauge-invariant operators because they give the same expectation values:

$$\langle \Phi | \hat{\mathcal{O}} | \Phi \rangle = (\langle \Phi | \hat{g}^{-1}) \hat{\mathcal{O}} (\hat{g} | \Phi \rangle) \quad \text{if } \hat{g}^{-1} \hat{\mathcal{O}} \hat{g} = \hat{\mathcal{O}}. \quad (9)$$

In principle, one can use a gauge-invariant state[30]

$$|\Phi; \text{inv}\rangle \equiv \mathcal{N}^{-1/2} \int_{\mathcal{G}} dg \hat{g} |\Phi\rangle, \quad (10)$$

where the normalization factor is

$$\mathcal{N} = \text{Vol}(\mathcal{G}) \int_{\mathcal{G}} dg \langle \Phi | \hat{g} | \Phi \rangle. \quad (11)$$

However, we obtain the same result anyway. To see this, note that the inner product of $|\Phi\rangle$ and $\hat{g}|\Phi\rangle$ is essentially the delta function $\delta(g - 1)$ because we are considering a well-localized wave packet whose width is much smaller than the typical values of $A_j^{(\text{cl.})}$. This is particularly so in physically meaningful setups of large lattice volume (which is the case in the continuum limit, even at fixed physical volume), because even a small transformation at each link accumulate to significant change that leads to vanishing overlap [31]. Furthermore, we are interested in ‘small’ operators, say a polynomial of field strength of a finite degree, which does not alter the wave packet significantly. To see this point in concrete terms, let x be the deviation of the coordinate variable A_j from its value at the center of the wave packet. The wave function is sharply peaked around $x = 0$. Suppose \hat{f} consists of several coordinate operators, say \hat{x}^k . Then, the wave function changes from $\Phi(x)$ to $x^k \Phi(x)$. Assuming that $\Phi(x)$ is localized (approximately) as $\Phi(x) \sim e^{-x^2/2\sigma^2}$ ($\sigma \ll 1$), and assuming k is finite (which is the meaning of ‘small’ here), $x^k \Phi(x)$ is also localized. If \hat{f} is also

gauge-invariant,

$$\begin{aligned} \langle \Phi; \text{inv} | \hat{f} | \Phi; \text{inv} \rangle &\simeq \mathcal{N}^{-1} \text{Vol}(\mathcal{G}) f(A^{\text{cl.}}) \int_{\mathcal{G}} dg \langle \Phi | \hat{g} | \Phi \rangle \\ &= f(A^{\text{cl.}}). \end{aligned} \quad (12)$$

For the same reason,

$$\langle \Phi | \hat{f} | \Phi \rangle \simeq f(A^{\text{cl.}}). \quad (13)$$

Therefore, we can use either the singlets or non-singlets; this is merely a matter of taste. In practice, however, it is common to use non-singlet states because it is more convenient to do so.

To make the point even clearer, it is instructive to consider a system of two identical, non-interacting bosons. As explained in Supplementary Material S1, this system has a gauge symmetry S_2 . Suppose that the state is obtained from two one-particle wave functions ϕ_1 and ϕ_2 with negligible overlap. Then, whether we use a non-singlet wave function $\phi_1(x_1)\phi_2(x_2)$ or singlet wave function $[\phi_1(x_1)\phi_2(x_2) + \phi_1(x_2)\phi_2(x_1)]/\sqrt{2}$, we obtain the same expectation value for singlet operators such as $\hat{x}_1^2 + \hat{x}_2^2$. This illustrates that physical content resides in gauge-equivalence classes, not in any particular representative. From this viewpoint, it is clear why we do not need to consider a fully symmetrized wave function of all identical bosons in the universe.

At the classical level, the equation of motion for A_t leads to the Gauss law constraint. Naively, the quantum counterpart to using the equation of motion for A_t would be to integrate out A_t , which, in turn, is equivalent to acting with a projector $\hat{\mathcal{P}}$ on quantum states (Supplementary Material S2). To see why the Gauss law matters, let us consider an open Wilson line connecting two spatial points \vec{x} and \vec{x}' , denoted by $\hat{W}(\vec{x}, \vec{x}')$ acting on the gauge-invariant ground state $|\text{VAC}\rangle$:

$$\hat{W}(\vec{x}, \vec{x}') |\text{VAC}\rangle. \quad (14)$$

There is no classical counterpart of such a state because it would violate the Gauss law. Such a state is projected to zero:

$$\hat{\mathcal{P}} \hat{W}(\vec{x}, \vec{x}') |\text{VAC}\rangle = 0. \quad (15)$$

Therefore, such a state is redundant. Of course, we can add fermions at the end points so that the Gauss law is satisfied. Namely, we can consider

$$\hat{\psi}(\vec{x}) \hat{W}(\vec{x}, \vec{x}') \hat{\psi}(\vec{x}') |\text{VAC}\rangle. \quad (16)$$

This state is gauge invariant, and the classical counterpart satisfies the Gauss law. Hence, one might think the Gauss law constraint in the classical theory should translate into the gauge invariance in the quantum theory; but that is not the case, as we can see from the following example [32] in the $SU(N)$ theory with fermions in the fundamental representation:

$$\hat{\psi}_a(\vec{x}) \hat{W}_{a,a'}(\vec{x}, \vec{x}') \hat{\psi}_{a'}(\vec{x}') |\text{VAC}\rangle. \quad (17)$$

Here, $a, a' = 1, 2, \dots, N$ are color indices, which are not summed over. Such a state is not gauge-invariant, but it satisfies the Gauss law in the sense that the color flux ends at sources, and it is not projected to zero:

$$\begin{aligned} \hat{\mathcal{P}} & \left(\hat{\psi}_a(\vec{x}) \hat{W}_{a,a'}(\vec{x}, \vec{x}') \hat{\psi}_{a'}(\vec{x}') |VAC\rangle \right) \\ & = \sum_{b,c=1}^N \hat{\psi}_b(\vec{x}) \hat{W}_{b,c}(\vec{x}, \vec{x}') \hat{\psi}_c(\vec{x}') |VAC\rangle. \end{aligned} \quad (18)$$

The right hand side $\sum_{b,c=1}^N \hat{\psi}_b(\vec{x}) \hat{W}_{b,c}(\vec{x}, \vec{x}') \hat{\psi}_c(\vec{x}') |VAC\rangle$ is obtained by averaging over the gauge orbit. $\hat{\psi}_a(\vec{x}) \hat{W}_{a,a'}(\vec{x}, \vec{x}') \hat{\psi}_{a'}(\vec{x}') |VAC\rangle$ is a particular choice of a representative element of this gauge orbit. To specify the orbit, we can use either the orbit itself or a representative element — there is no difference in the information in our hands. The same holds for closed strings. Namely,

$$\hat{W}_{\text{closed}}^{(\text{singlet})} \equiv \text{Tr}(\hat{Z}_{j_1, \vec{x}} \hat{Z}_{j_2, \vec{x}+\hat{j}_1} \cdots \hat{Z}_{j_l, \vec{x}-\hat{j}_l}) \quad (19)$$

and

$$\hat{W}_{\text{closed}}^{(\text{non-singlet})} \equiv N^l \hat{Z}_{j_1, \vec{x}; a_1 a_2} \hat{Z}_{j_2, \vec{x}+\hat{j}_1; a_2 a_3} \cdots \hat{Z}_{j_l, \vec{x}-\hat{j}_l; a_l a_1} \quad (20)$$

carry the same information. Note that the joining/splitting interactions between strings (Fig. 1) are described in the same manner in both singlet and non-singlet descriptions, as we show in Appendix A 3.

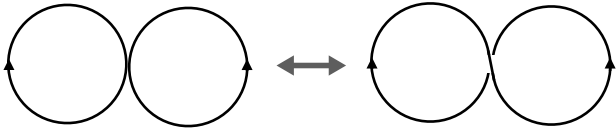


FIG. 1. Joining/splitting interactions of strings.

We can also create a redundant state, which is analogous to BRST-exact states, by taking a difference between two elements on the orbit, e.g., $\hat{\psi}_1(\vec{x}) \hat{W}_{1,1}(\vec{x}, \vec{x}') \hat{\psi}_1(\vec{x}') |VAC\rangle - \hat{\psi}_2(\vec{x}) \hat{W}_{2,2}(\vec{x}, \vec{x}') \hat{\psi}_2(\vec{x}') |VAC\rangle$. For unitary link variables, ‘whiskers’ such as $\hat{U}_{j,\vec{n}}^{ab} \hat{U}_{j,\vec{n}}^{\dagger bc}$ are projected to the identity matrix, and hence $\hat{W}^{(\text{non-singlet})}$ with and without whiskers (see Figure 2) are physically equivalent. In this case, it is more reasonable to use a loop without whiskers.

When one considers thermodynamics, it would be good to use singlet states to avoid over-counting. If one is interested in a microstate, such as the Hamiltonian time evolution of a specific initial condition, then either the singlet or the non-singlet can work, depending on the details of the task. In fact, even a redundant state — an element of $\text{Ker}(\hat{\mathcal{P}})$ — may be fine. For a well-localized wave packet $|\Psi\rangle$, we can define a redundant state $(|\Phi\rangle -$

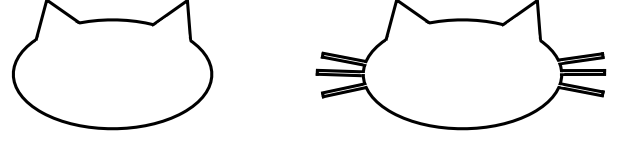


FIG. 2. Wilson loops with and without whiskers. For Kogut-Susskind, whiskers disappear (in other words, they become **1**) after the singlet projection. The difference between $\hat{W}^{(\text{non-singlet})}$ with and without whiskers is in $\text{Ker}(\hat{\mathcal{P}})$ and thus redundant. With or without whiskers, a cat is a cat!

$\hat{g}|\Phi\rangle)/\sqrt{2}$. If $|\Phi\rangle$ and $\hat{g}|\Phi\rangle$ are sufficiently separated and a gauge-invariant operator \hat{O} does not mix them, then the expectation value of \hat{O} is the same whether we use $|\Phi\rangle$, $\hat{g}|\Phi\rangle$, or $(|\Phi\rangle - \hat{g}|\Phi\rangle)/\sqrt{2}$.

III. QUANTUM SIMULATIONS WITH SINGLET CONSTRAINT

From here on, we consider circuit implementations. We will use the orbifold lattice Hamiltonian (Appendix B) and the universal framework [21] (see also Supplementary Material S3) that allows us to construct quantum circuits explicitly. Combined with our previous work [21, 23], this section completes efficient quantum simulation method for Yang-Mills theory and QCD with gauge-singlet constraint.

Conceptually, the simplest way to achieve quantum simulation with the gauge-singlet constraint is to explicitly construct the projection procedure from \mathcal{H}_{ext} to \mathcal{H}_{inv} [33]. Such a procedure is characterized by its action on the coordinate eigenstate. Specifically, it must transform $|Z\rangle$ into $\int d\Omega |Z^{(\Omega)}\rangle$, where the integral is taken over the Haar measure. Note that such a procedure is not realizable by a unitary operator acting on the Hilbert space, because many non-singlets correspond to one singlet.

Our protocol consists of the following steps:

- **Step 1.** Create operators $\hat{\xi}_{\vec{n}}$ and states $|\xi\rangle = \otimes_{\vec{n}} |\xi_{\vec{n}}\rangle$ satisfying $\hat{\xi}_{\vec{n}} |\xi_{\vec{n}}\rangle = \xi_{\vec{n}} |\xi_{\vec{n}}\rangle$, where $\xi_{\vec{n}} \in \mathbb{C}^{N \times N}$.
- **Step 2.** Produce $|Z^{(\xi)}\rangle |\xi\rangle$ from $|Z\rangle |\xi\rangle$, where $Z_{j,\vec{n}}^{(\xi)} = \xi_{\vec{n}} Z_{j,\vec{n}} \bar{\xi}_{\vec{n}+\hat{j}}$.
- **Step 3.** Take an average over $\xi_{\vec{n}} \in \text{SU}(N) \subset \mathbb{C}^{N \times N}$.

Step 1. We can introduce a complex matrix $\xi_{\vec{n}} \in \mathbb{C}^{N \times N}$ and ancilla states $|\xi\rangle = \otimes_{\vec{n}} |\xi_{\vec{n}}\rangle$ just by using the techniques in the orbifold lattice formulation. We assign Q qubits for each bosonic degree of freedom. (In principle, we can assign different number than Q .)

Step 2. To shift $|Z\rangle$ to $|Z^{(\xi)}\rangle$, we can use

$$\langle P|Z\rangle = \exp \left(-i \sum_{j,\vec{n}} \text{Tr} [P_{j,\vec{n}} \bar{Z}_{j,\vec{n}} + \bar{P}_{j,\vec{n}} Z_{j,\vec{n}}] \right) \quad (21)$$

and a similar equation for $|Z^{(\xi)}\rangle$, which give us

$$\begin{aligned} |Z^{(\xi)}\rangle &= \int dP |P\rangle \langle P|Z\rangle \\ &\times \exp \left(i \sum_{j,\vec{n}} \text{Tr} [P_{j,\vec{n}} (\bar{Z}_{j,\vec{n}} - \bar{Z}_{j,\vec{n}}^{(\xi)}) \right. \\ &\left. + \bar{P}_{j,\vec{n}} (Z_{j,\vec{n}} - Z_{j,\vec{n}}^{(\xi)})] \right). \end{aligned} \quad (22)$$

Note also that, by using

$$\hat{Z}_{j,\vec{n}}^{(\xi)} \equiv \hat{\xi}_{\vec{n}} \hat{Z}_{j,\vec{n}} \hat{\xi}_{\vec{n}+\vec{j}}, \quad (23)$$

we have

$$\hat{Z}^{(\xi)} |Z\rangle |\xi\rangle = Z^{(\xi)} |Z\rangle |\xi\rangle. \quad (24)$$

To produce $|Z^{(\xi)}\rangle$ using this operator, firstly we create $\int dZ F(Z) |Z\rangle_1 |Z\rangle_2 |\xi\rangle$ from $\int dZ F(Z) |Z\rangle_1 |\xi\rangle$. Here, we used a subscript to distinguish two copies. This straightforward because $|Z\rangle$ is binary; we just tensor $|0,0,\dots,0\rangle_2$ and act CNOT gates. Now, we define a new unitary operator:

$$\hat{\mathcal{T}}^{(\xi)} \equiv \exp \left(i \text{Tr} [\hat{P}_1 (\hat{Z}_2 - \hat{Z}_2^{(\xi)}) + \hat{P}_1 (\hat{Z}_2 - \hat{Z}_2^{(\xi)})] \right). \quad (25)$$

Here, \hat{P}_1 and $\hat{\mathcal{T}}^{(\xi)}$ acts on $|Z\rangle_1$, \hat{Z}_2 and $\hat{\mathcal{T}}^{(\xi)}$ acts on $|Z\rangle_2$, and $\hat{Z}_2^{(\xi)}$ is made of \hat{Z}_2 and $\hat{\xi}$. (We did not write j, \vec{n} explicitly just to avoid cluttered notations.) Note that all operators inside the exponential commute with each other and hence there is no ordering ambiguity. Using this operator, we can easily see that [34]

$$\hat{\mathcal{T}}^{(\xi)} |Z\rangle_1 |Z\rangle_2 |\xi\rangle = |Z^{(\xi)}\rangle_1 |Z\rangle_2 |\xi\rangle. \quad (26)$$

By seeing $\text{Tr} [\hat{P}_1 (\hat{Z}_2 - \hat{Z}_2^{(\xi)}) + \hat{P}_1 (\hat{Z}_2 - \hat{Z}_2^{(\xi)})]$ as ‘Hamiltonian’, we can regard $\hat{\mathcal{T}}^{(\xi)}$ as ‘Hamiltonian time evolution’. By performing the Quantum Fourier Transform to $|Z\rangle_1$ and going to the momentum basis, \hat{P}_1 and $\hat{\mathcal{T}}^{(\xi)}$ becomes a sum of Pauli σ_z s. The other operators (\hat{Z}_2 , $\hat{Z}_2^{(\xi)}$, $\hat{\mathcal{T}}^{(\xi)}$) are also written using Pauli σ_z s. Therefore, we can use the universal framework [21] (see also Supplementary Material S3 A).

Now we need to eliminate $|Z\rangle_2$. An expensive but precise method is to project it to $\frac{1}{2^{N^2 Q}} (\sum_{Z'} |Z'\rangle_2)$. We can simply perform measurement in $|\pm\rangle = \frac{|0\rangle \pm |1\rangle}{\sqrt{2}}$ basis or use amplitude amplification. Either way, the cost scaling is

exponential in $N^2 Q$. A better method is to act another operator,

$$\hat{\mathcal{T}}'^{(\xi)} \equiv \exp \left(i \text{Tr} [\hat{P}_2 \hat{\mathcal{Z}}_1^{(\bar{\xi})} + \hat{P}_2 \hat{\mathcal{Z}}_1^{(\bar{\xi})}] \right). \quad (27)$$

Then, $\hat{\mathcal{Z}}_1^{(\bar{\xi})}$ acting on $|Z^{(\xi)}\rangle_1$ picks up $Z^{(\bar{\xi}\xi)}$. In the infinite mass limit, ξ is unitary, and $\bar{\xi}$ is ξ^{-1} , and hence, $Z^{(\bar{\xi}\xi)} = Z$. Therefore, by acting $\hat{\mathcal{T}}'^{(\xi)}$, $|Z\rangle_2$ is approximately sent to $|Z=0\rangle_2$, which allows us more reliable projection with a higher probability. Either way, we use $(\hat{\mathcal{T}}^{(\xi)} |Z\rangle_1 |Z\rangle_2 |\mathcal{G}\rangle)_{\text{proj.}}$ to denote the state after projecting out $|Z\rangle_2$. Note that, even if we improve the success probability of post selection in this way, repeated post-selection leads to exponentially large cost in general.

Step 3. We prepare a state $|\mathcal{G}\rangle = \int d\xi \varphi(\xi) |\xi\rangle$ in such a way that $|\mathcal{G}\rangle$ is a linear combination of $\xi_{\vec{n}} \in \text{SU}(N)$ with Haar measure. Equivalently, $\varphi(\xi)$ is $\text{SU}(N)$ -invariant and vanishes quickly as ξ departs from $\text{SU}(N) \in \mathbb{C}^{N \times N}$. There exist many ways to build $|\mathcal{G}\rangle$. One way is to multiply $\exp(-C \text{Tr}(\hat{\xi} \hat{\xi} - \mathbf{1})^2)$ and $\exp(-C' |\det \hat{\xi} - 1|^2)$ to a state proportional to $\sum_{\xi} |\xi\rangle$, where C and C' are large positive numbers. As discussed in Supplementary Material S5, this is straightforward by using the Linear Combination of Unitaries (LCU; see Supplementary Material S4) or Quantum Singular Value Transform (QSVT). Another natural option would be to minimize a Hamiltonian

$$\hat{H}_{\xi} = \text{Tr} \hat{P}_{\xi} \hat{\mathcal{P}}_{\xi} + c_1 \cdot \text{Tr} (\hat{\xi} \hat{\xi} - \mathbf{1})^2 + c_2 \cdot |\det \hat{\xi} - 1|^2 \quad (28)$$

with large coefficients c_1 and c_2 . In the limit of $c_1 \rightarrow \infty$, ξ is forced to be unitary, and in the limit of $c_2 \rightarrow \infty$, determinant becomes 1. The momentum part makes the distribution uniform along the $\text{SU}(N)$ group manifold. See Sec. V for numerical demonstration of this approach. By using $|\mathcal{G}\rangle$, we can realize the average over $\text{SU}(N)$:

$$\langle \mathcal{G} | (\hat{\mathcal{T}}^{(\xi)} |Z\rangle_1 |Z\rangle_2 |\mathcal{G}\rangle)_{\text{proj.}} = \int_{\text{SU}(N)} d\Omega |Z^{(\Omega)}\rangle. \quad (29)$$

This projection involves a post-selection, which, again, can lead to exponentially large cost if the projection is repeated multiple times.

Supplementary Material S5 provides more details of the computations in this section.

IV. QUANTUM SIMULATIONS WITHOUT SINGLET CONSTRAINT

In Sec. II, we emphasized the importance of a non-singlet description of gauge-invariant physics, taking electromagnetism as an example. Specifically, a ‘physical state’ can be described using either a singlet or a non-singlet, and certain simple types of the latter, such as

a wave packet, are conceptually and technically easier. Here, we are talking about a “wave packet” in the field space, i.e., gauge field $A_\mu(x)$ is localized at each spatial point x . In the lattice theory, it is a wave packet on the group manifold. This is a rather fundamental class; for example, the ground state is a wave packet around $U = 1$ (and also $W = 1$, for the case of the orbifold lattice), up to gauge transformation.

In this section, we focus on the practical utility of the non-singlet description in quantum simulations. We consider two options: non-singlet-string excitation on a gauge-invariant state, and a wave packet. The use of the non-singlet description can be useful to avoid cost of the singlet projection introduce in Sec. III whenever possible.

A. Non-singlet strings

Suppose that the gauge-invariant ground state is already prepared. We can act with non-singlet operators on it to obtain non-singlet states. For example, we consider closed strings (Wilson loops) and open strings (Wilson lines). For many cases of interest, we obtain the same result whether we use singlets or non-singlets.

To understand the concepts, we can use the vanilla Kogut-Susskind or orbifold lattice formulation; The details do not matter, unless one considers the circuit implementation, which is much more efficient for the orbifold formulation. Below, we use the orbifold lattice for concreteness.

Gauge-invariant states in \mathcal{H}_{inv} can be obtained by acting with Wilson loop operators (often called closed strings) \hat{W}_{closed} defined by (19) on $|\text{VAC}\rangle$. The number of terms in the sum increases exponentially with the length of the loop l as N^l . When N or l is large, it is better to avoid such an increase.

A simple way to avoid such an increase is to use non-singlet states [35]. Suppose that no loop intersects with other loops or with itself. Then, such an operator is obtained by symmetrizing $\hat{W}_{\text{closed}}^{(\text{non-singlet})}$ defined by (20). Note that, in this case, symmetrization over $\text{SU}(N)$ is the same as taking the average over all possible choices of a_1, \dots, a_l . Using $\hat{W}^{(\text{singlet})}$ or $\hat{W}^{(\text{non-singlet})}$ does not make a difference in the following case. Suppose that $|\text{VAC}\rangle$ is gauge invariant. Let us consider a correlation function of multiple loops $\hat{W}_1^{(\text{singlet})}, \dots, \hat{W}_n^{(\text{singlet})}$. If all loops are spatially separated,

$$\begin{aligned} \langle \text{VAC} | \hat{W}_1^{(\text{singlet})} e^{-it_1 \hat{H}} \hat{W}_2^{(\text{singlet})} e^{-it_2 \hat{H}} \dots \\ \dots e^{-it_{n-1} \hat{H}} \hat{W}_n^{(\text{singlet})} | \text{VAC} \rangle \\ = \langle \text{VAC} | \hat{W}_1^{(\text{non-singlet})} e^{-it_1 \hat{H}} \hat{W}_2^{(\text{non-singlet})} e^{-it_2 \hat{H}} \dots \\ \dots e^{-it_{n-1} \hat{H}} \hat{W}_n^{(\text{non-singlet})} | \text{VAC} \rangle. \end{aligned} \quad (30)$$

(This can be seen using $\mathcal{P}|\text{VAC}\rangle = |\text{VAC}\rangle$, $\langle \text{VAC} | \mathcal{P} = \langle \text{VAC}|$, and projection properties explained in Sec. II C.) In this way, singlet and non-singlet descriptions can lead to the same result.

Note that the same holds for the lattice Monte Carlo simulation on classical computers: if configurations are generated without gauge fixing (analogous to the use of a gauge-invariant ground state $|\text{VAC}\rangle$), we obtain the same expectation values for $\hat{W}^{(\text{singlet})}$ and $\hat{W}^{(\text{non-singlet})}$.

Although the same expectation value is guaranteed, more measurements might be needed to estimate the expectation value precisely when the non-singlet states are used. Still, the non-singlet description can simplify the circuit implementations, and also, it can provide some conceptual advantages when certain problems are considered, as mentioned at the beginning of this section.

Preparation of string states

Let us consider closed strings. (Open strings are similar.) Whether we use the singlet version like $\hat{W}^{(\text{singlet})}$ or non-singlet version like $\hat{W}^{(\text{non-singlet})}$, they are written as a sum of Pauli strings made of only σ_z s with length l , because each \hat{Z} is a sum of σ_z s. The number of Pauli strings scales as $(2Q)^l$ for $\hat{W}^{(\text{non-singlet})}$ and $(2NQ)^l$ for $\hat{W}^{(\text{singlet})}$. (The relative factor N^l gives us a strong motivation to use non-singlet states. In case we prefer singlet states, we can compute traces explicitly, or use the projection method in Sec. III, or use yet another method in Supplementary Material S4.) That we have a simple Pauli string expansion makes state preparation straightforward.

Let us consider a method based on LCU (Supplementary Material S4). The task is, for a given state $|\Phi\rangle$ (say the ground state), to obtain $\frac{\hat{O}|\Phi\rangle}{\|\hat{O}|\Phi\rangle\|}$, where \hat{O} is $\hat{W}^{(\text{singlet})}$ or $\hat{W}^{(\text{non-singlet})}$. For this purpose, we can apply the LCU method (as reviewed in Supplementary Material S4) directly without modification, because the Pauli-string expansion of the following form is known explicitly:

$$\hat{O} = \sum_i \alpha_i \hat{\Pi}_i. \quad (31)$$

Note that we can take all α_i real and non-negative, attributing the phase to $\hat{\Pi}_i$. As long as the loop consists of a finite number of links, $\sum_i |\alpha_i|$ is bounded.

B. Wave packet

Let us use a wave packet as discussed in Sec. II. If we consider the ground state at weak coupling [36], a wave packet localized around $W_{j,\vec{n}} = \mathbf{1}_N$ and $U_{j,\vec{n}} = \mathbf{1}_N$, which we denote by $|\Phi\rangle$, describes the ground state. Such a wave packet is not gauge invariant; any wave packet equivalent to $|\Phi\rangle$ up to a gauge transformation has the same property. A gauge transformation by $\Omega \in \mathcal{G}$ maps $|\Phi\rangle$ to $\hat{\Omega}|\Phi\rangle$, which is a wave packet localized around $W_{j,\vec{n}} = \mathbf{1}_N$ and $U_{j,\vec{n}} = \Omega_{\vec{n}} \Omega_{\vec{n}+j}^{-1}$. Hence $|\Phi\rangle$ can be invariant only under the global $\text{SU}(N)$ transformation. The

gauge-invariant ground state is obtained by projection, as we saw in Sec. II.

To take the continuum limit, the lattice spacing a and coupling constant g are sent to zero, and the lattice size is sent to infinity. In this limit, $\langle \Phi | \hat{\Omega} | \Phi \rangle$ is essentially a product of delta functions, $\prod_{\vec{n}} \delta(\Omega_{\vec{n}} \Omega_{\vec{n}+\hat{j}}^{-1} - \mathbf{1}_N)$. This is because $|\Phi\rangle$ and $\hat{\Omega}|\Phi\rangle$ can have a non-negligible overlap only when the overlap is almost perfect at all sites (i.e., $\Omega_{\vec{n}} \Omega_{\vec{n}+\hat{j}}^{-1}$ is very close to $\mathbf{1}_N$ at all \vec{n}).

A natural strategy for quantum simulations is to act with gauge-singlet operators on this non-singlet state, as we discussed for classical electromagnetism in Sec. II.

To obtain a wave packet localized around $W = 0$ and $U = \mathbf{1}_N$, we can add a penalty term proportional to

$$\sum_{\vec{n}} \sum_{j=1}^3 \text{Tr} \left| \langle \hat{Z}_{j,\vec{n}} \rangle - \sqrt{\frac{a}{2g^2}} \cdot \mathbf{1}_N \right|^2. \quad (32)$$

Alternatively, we might be able to use the adiabatic state preparation method, starting with a special point in the orbifold lattice where the ground state can be obtained analytically (e.g., the weak-coupling limit) and then changing the parameters adiabatically. Whether this approach works depends on the structure of the phase diagram, which can be studied using the standard Euclidean path integral.

When using LCU and Taylor expansion, imaginary time evolution is straightforward.

V. VALIDATION OF CONVERGENCE CRITERIA

We validate our framework through systematic numerical studies on classical computers. This approach allows exact verification of algorithm correctness, convergence criteria, and scaling properties at system sizes where analytical results or exact diagonalization provide ground truth. Classical validation is the appropriate methodology for algorithm verification; quantum hardware becomes relevant when system sizes exceed classical simulation capabilities, where our validated scaling ensures quantum advantage.

In this section, we will focus on the truncation effect and Trotter scaling for the mass terms that enforce unitarity constraints. We first provide a theoretical analysis that holds regardless of the details of the interactions, dimensions, and lattice size, and then we provide numerical demonstrations on classical computers using small systems. The validation conducted in this section is relevant both for the singlet-projection protocol introduced in Sec. III and other parts of the universal simulation protocol [21] (see also Supplementary Material S3).

To write an efficient quantum circuit for gauge theory, the use of non-compact variables (complex link variable $Z_{j,\vec{n}}$, and a complex matrix ξ to express the $SU(N)$ gauge transformation in Sec. III) was crucial. Furthermore, the state $|\mathcal{G}\rangle$, which play the crucial role in the

singlet-projection protocol introduced in Sec. III, could be described as the ground state of the Hamiltonian (28), which is actually an embedding of strongly-coupled lattice gauge theory into noncompact variables, as we will see below. Natural questions associated with this approach are: how many qubits do we need to express unitary variables precisely? How large a mass do we need if we want to remove the scalars so that the orbifold lattice Hamiltonian reduces to the Kogut-Susskind Hamiltonian? Does a large mass in such a limit affect the simulation cost? In this section, we address these questions by numerical experiments on classical computers.

Numerically demonstrating convergence criteria using classical computers is challenging — that is the very reason why we do need a quantum computer! To reduce the computational cost for a demonstration, we consider the counterpart of the strong-coupling limit of the Kogut-Susskind Hamiltonian. Specifically, we drop the second and third lines in the orbifold lattice Hamiltonian (B8), keeping the kinetic term $\sum_{j,\vec{n}} \text{Tr} \hat{P}_{j,\vec{n}} \hat{P}_{j,\vec{n}}$ and the mass term \hat{H}_{mass} defined by (B9). Then, there is no interaction between different sets of (j, \vec{n}) . Therefore, we can focus on a single link and consider the following Hamiltonian:

$$\hat{H} = \text{Tr} \hat{P} \hat{P} + \hat{H}^{(\text{mass})}, \quad (33)$$

$$\hat{H}^{(\text{mass})} = \text{Tr} \left(m^2 \left(\hat{Z} \hat{Z} - \mathbf{1}_N \right)^2 + m_{U(1)}^2 |\det \hat{Z} - 1|^2 \right). \quad (34)$$

Here, to simplify the expression, we set g^2 and a to 1.

We want to see the behavior of this model in the infinite-mass limit. This is still a challenging task because the $SU(N)$ group manifold is embedded into $\mathbb{C}^{N^2} = \mathbb{R}^{2N^2}$ and the dimension of the truncated Hilbert space is Λ^{2N^2} . Here, Λ is the truncation level for each boson. It is easy to see that the dimension of the truncated Hilbert space grows fast even for $N = 2$. Hence, let us simplify the problem without losing the essence, in the following manner.

For $N = 2$, the constraint imposed by the mass term can be written as $\vec{v}_i^\dagger \vec{v}_j = \delta_{ij}$, where v_i are column vectors (i.e., $Z = (\vec{v}_1, \vec{v}_2)$), and $\det Z = 1$. Among them, let us first impose $\vec{v}_1^\dagger \vec{v}_2 = 0$, $|\vec{v}_1|^2 = |\vec{v}_2|^2$, and $\det Z \in \mathbb{R}$. This can be achieved by arranging the mass term appropriately and sending the mass parameter corresponding to these constraints to large values. Then, the complex matrix Z becomes

$$Z = \begin{pmatrix} \alpha & -\beta^* \\ \beta & \alpha^* \end{pmatrix} \quad \alpha, \beta \in \mathbb{C}. \quad (35)$$

Note that $Z \in SU(2)$ when the remaining constraint $|\alpha|^2 + |\beta|^2 = 1$ is imposed. This gives the embedding of $SU(2) = S^3$ into \mathbb{R}^4 . By writing this Z as $Z = e^\phi U$, we can interpret ϕ and U as a scalar and $SU(2)$ link variable, respectively. To get $SU(2)$, we remove ϕ by taking its mass large.

This is a special case of the standard embedding of S^n into \mathbb{R}^{n+1} . As a counterpart of (33), we will study the following Hamiltonian consisting of $n+1$ bosons:

$$\hat{H} = \frac{1}{2} \sum_{a=1}^{n+1} \hat{p}_a^2 + \frac{m^2}{8} \left(\sum_{a=1}^{n+1} \hat{x}_a^2 - 1 \right)^2. \quad (36)$$

Interpreting the radial coordinate as a scalar ϕ , i.e., $\sum_{a=1}^{n+1} x_a^2 = e^{2\phi}$, the second term is the scalar mass term $\frac{m^2}{2}\phi^2$. When mass is large, ϕ vanishes, and the low-energy states are restricted to the unit sphere S^n . This is the same mechanism as that for the $SU(N)$ embedded into \mathbb{R}^{2N^2} . For $n=3$, we obtain the example of the orbifold lattice discussed above. For $n=1$, we obtain $U(1)$ embedded into $\mathbb{C} = \mathbb{R}^2$. Note that, for $SU(2)$, this setup (four bosons per link) is likely to be more useful for quantum simulations than the original formulation (eight bosons per link) because the number of qubits and quantum gates necessary for quantum simulations can be reduced significantly.

This setup makes the numerical test tractable with a laptop for $n=1, 2$, and 3 . As we show in Supplementary Material S5, this gives a testbed for the singlet-projection protocol discussed in Sec. III, too.

We take m^2 large and focus on the low-energy states. Then, ϕ behaves as a harmonic oscillator decoupled from the S^n part, as in the case of scalars in the orbifold lattice Hamiltonian. The ground-state wave function is proportional to $\exp\left(-\frac{m\phi^2}{2}\right)$, whose width scales as $1/\sqrt{m}$ with m . Namely, the sphere created by the scalar mass term has a thickness of order $\frac{1}{\sqrt{m}}$. For a good approximation of the low-energy modes, we need sufficiently many points in this width, and hence,

$$\delta_x = \frac{2R}{\Lambda} \lesssim \frac{1}{\sqrt{m}} \quad (37)$$

is needed. We can derive the same convergence criterion for the orbifold lattice, when the Kogut-Susskind limit is considered taking m larger than a^{-1} . Note that this estimate holds regardless of the details of the interactions, dimensions, and lattice size.

The numerical studies below confirm this theoretical scaling and demonstrate that the convergence is rapid and controllable in practice.

A. Ground-state wave function

Let $\psi_{\text{g.s.}}(x_1, x_2)$ be the ground-state wave function. In Fig. 3, $|\psi_{\text{g.s.}}(x_1, x_2)|^2$ is shown for $m=40$, $R=2$, and $\Lambda=32, 64$. The wave function is normalized to match the limit of $\Lambda \rightarrow \infty$, dividing by δ_x^2 . The distribution is a thin ring close to S^1 , as it should be.

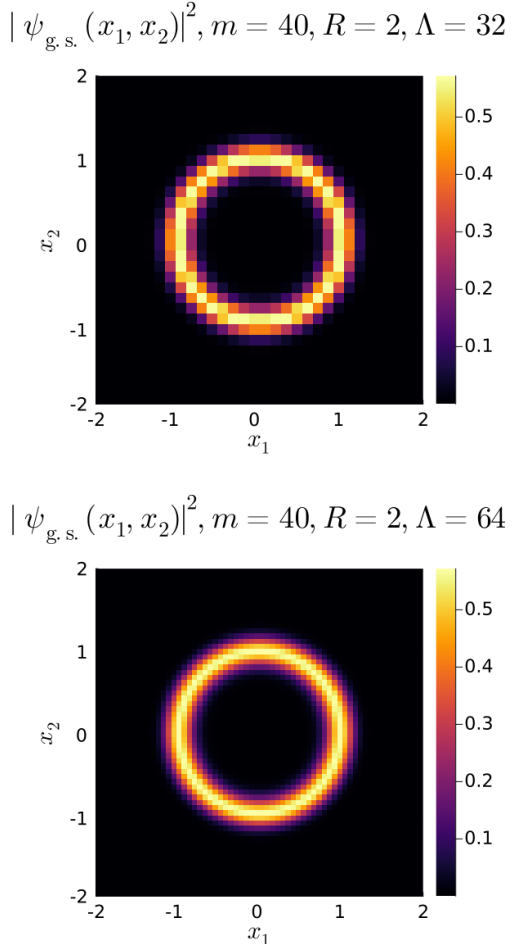


FIG. 3. The square of the ground-state wave function for the $n=1$ model, $|\psi_{\text{g.s.}}(x_1, x_2)|^2$. We used $m=40$, $R=2$, and $\Lambda=32, 64$.

B. Energy spectrum

We study the energy spectrum varying the scalar mass m^2 and truncation level Λ , while fixing R to be 2.0.

$n=1$ model. In the energy spectrum, we can see non-degenerate eigenvalues that correspond to zero modes along the $U(1)$ direction and two-fold-degenerate eigenvalues that correspond to nonzero momentum along the $U(1)$ direction. In Table III, we show the first and second non-degenerate energy levels, with $R=2.0$ and $\Lambda=64$, for $m=10, 20, 30$, and 40 . The first one is always E_0 , as expected. We can see the approach to the harmonic oscillator values, $\frac{m}{2}$ and $\frac{3m}{2}$.

For sufficiently large m , low-lying modes correspond to the excitations along the $U(1)$ direction. $E_1 = E_2$, $E_3 = E_4$, and $E_5 = E_6$ correspond to momentum $p = \pm 1, \pm 2$, and ± 3 , respectively. The difference from E_0 should be $\frac{p^2}{2}$ in the infinite-mass limit. We demonstrated this in Fig. 4.

In Fig. 5, we showed how the low-energy spectrum depends on δ_x . We observe roughly the same amount of corrections at $\sqrt{m}\delta_x$. Therefore, as expected, we can control the corrections by taking $\delta_x \lesssim \frac{1}{\sqrt{m}}$.

m	E_0	2nd non-degenerate level
10	4.503	12.437
20	9.582	27.712
30	14.599	42.903
40	19.606	57.971

TABLE III. The first and second non-degenerate energy levels, with $R = 2.0$ and $\Lambda = 64$, for $m = 10, 20, 30$, and 40 . The first one is always E_0 , as expected. We can see the approach to the harmonic oscillator values, $\frac{m}{2}$ and $\frac{3m}{2}$. The $n = 1$ model.

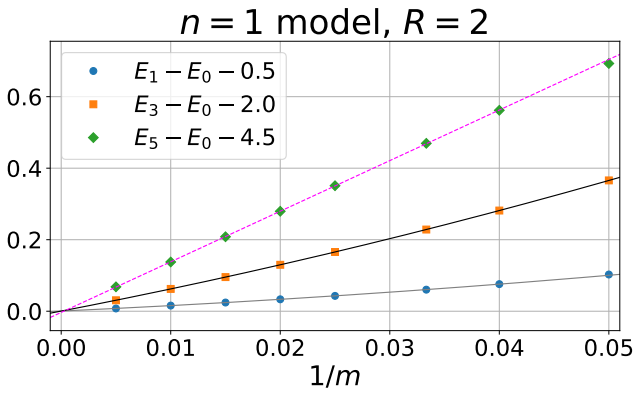


FIG. 4. For the $n = 1$ model, the difference between E_0 and two-fold degenerate states corresponding to momentum $p = \pm 1, \pm 2$, and ± 3 along the $U(1)$ direction should be $\frac{p^2}{2}$ in the infinite-mass limit. Specifically, $E_1 - E_0 - 0.5$, $E_3 - E_0 - 2.0$, and $E_5 - E_0 - 4.5$ should converge to zero. We plotted these numbers for several values of m between 20 and 200. The lines are quadratic fit with respect to $1/m$. We used $R = 2$, and Λ was take sufficiently large so that the error is less than 10^{-5} .

$n = 2$ model. When the mass is large, the energy can be approximated by the contributions from the Laplacian on S^2 and the harmonic oscillator describing a small fluctuation of the scalar. The former provides $\frac{1}{2}j(j+1)$, $j = 0, 1, 2, \dots$, with degeneracy $2j+1$. The latter adds $(\frac{1}{2}+k)m$, $k = 0, 1, 2, \dots$. In Fig. 6, we took $m = 40$ and $R = 2$, and plotted $E_\ell - E_0$ for $0 \leq \ell < 100$, taking the truncation level $\Lambda = 16, 20$, and 24 . We also show the ‘approximation’ explained above. We can see a quick convergence as Λ increases, and the large- Λ result is close to the ‘approximation’.

Fig. 7 shows that the Laplacian on S^2 is obtained precisely in the infinite-mass limit. Specifically, we showed that the differences between the first three groups of de-

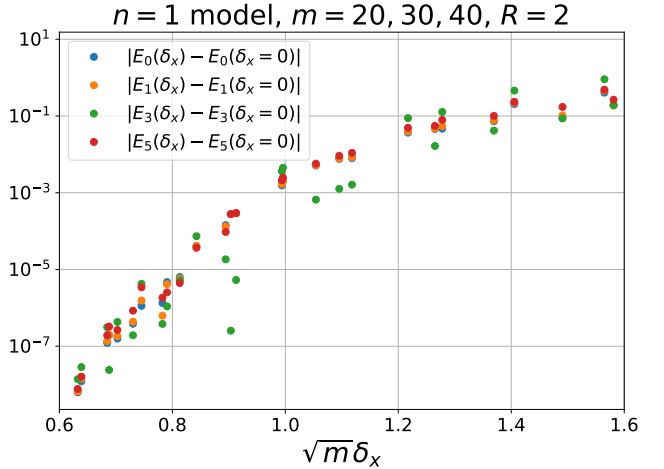


FIG. 5. For the $n = 1$ model at $R = 2$ and $m = 20, 30$, and 40 , the low-lying spectrum was calculated varying Λ (and hence $\delta_x = 2R/\Lambda$), and the difference from the values at $\delta_x = 0$ was plotted. The energy eigenvalues at $\delta_x = 0$ were estimated using sufficiently small δ_x where so that the error is smaller than 10^{-10} . By using $\sqrt{m}\delta_x$ as the horizontal axis, results from different mass line up and show the same exponential decay. This means we should take $\delta_x \lesssim \frac{1}{\sqrt{m}}$ to approximate the spectrum well. Note that we plotted the absolute value $|E_\ell(\delta_x) - E_\ell(\delta_x = 0)|$ because the sign oscillates.

generate eigenvalues and E_0 ($E_1 - E_0$, $E_4 - E_0$, and $E_9 - E_0$) converge to the values consistent with the values obtained from the Laplacian on S^2 (1.0, 3.0, and 6.0).

In Fig. 8, we showed how the low-energy spectrum depends on δ_x . We observe roughly the same amount of corrections at $\sqrt{m}\delta_x$. Therefore, as expected, we can control the corrections by taking $\delta_x \lesssim \frac{1}{\sqrt{m}}$.

$n = 3$ model. The Laplacian on $S^3 = SU(2)$ provides $\frac{1}{2}j(j+2)$, $j = 0, 1, 2, \dots$, with degeneracy $(j+1)^2$. The latter adds $(\frac{1}{2}+k)m$, $k = 0, 1, 2, \dots$. In Fig. 9, we took $m = 40$ and $R = 1.5$, and plotted $E_\ell - E_0$ for $0 \leq \ell < 100$, taking the truncation level $\Lambda = 8, 12$, and 16 . We also show the ‘approximation’ explained above. Note that the excited modes of the scalar ($k \geq 1$) do not appear in this range. We can see a quick convergence as Λ increases, and that the large- Λ result is close to the ‘approximation’. The correct degeneracy pattern shows that the structure of the $SU(2)$ group manifold is properly captured. Therefore, we conclude that the ground state serves as the state $|\mathcal{G}\rangle$, which play the crucial role in the singlet-projection protocol introduced in Sec. III, and can be systematically improved by taking m and Λ larger.

C. Numerical demonstration for singlet projection

Next, we study how the Hilbert space truncation affects the singlet projection. (Supplementary Mate-

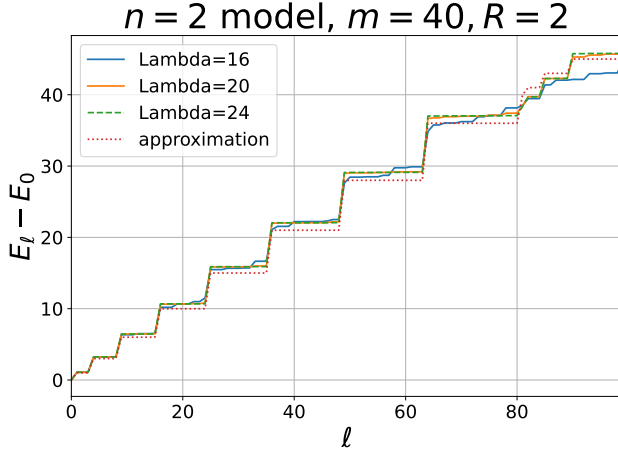


FIG. 6. $E_\ell - E_0$ ($0 \leq \ell < 100$) for the $n = 2$ model, $m = 40$, $R = 2$. An ‘approximation’ is obtained assuming that the spectrum is a sum of the contribution from the Laplacian on S^2 and a harmonic oscillator describing the radial coordinate, without interaction. Such an approximation is good when m is large.

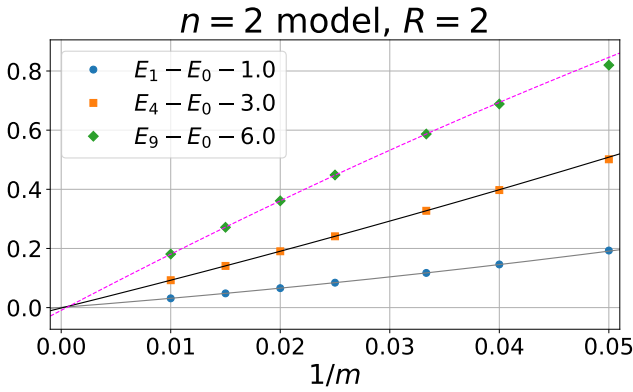


FIG. 7. For the $n = 2$ model, $E_1 - E_0 - 1$, $E_4 - E_0 - 3$, $E_9 - E_0 - 6$, which should converge to zero as $m \rightarrow \infty$, are plotted. We plotted these numbers for several values of m between 20 and 100. The lines are quadratic fit with respect to $1/m$. We used $R = 2$, and Λ was taken sufficiently large so that the error is smaller than 10^{-3} .

rial S5B gives further details.) A reasonable measure of the truncation effect is

$$\langle Z \rangle_{\text{proj.}} \hat{G}_{\text{truncated}}^2 |Z\rangle_{\text{proj.}}, \quad (38)$$

where $|Z\rangle_{\text{proj.}}$ is the projected version of the singlet-projected state and $\hat{G}_{\text{truncated}}$ is the truncated version of the $SU(N)$ generators.

Numerical evaluation of this quantity requires a large cost. As a tractable case, let us consider $U(1)$ embedded into $\mathbb{C} = \mathbb{R}^2$, and just one link. The Hilbert space is a truncated version of $\text{Span}\{|z\rangle \mid z \in \mathbb{C}\}$. We take $z = (x + iy)/\sqrt{2}$, and restrict x and y to $\pm\delta_x/2, \pm 3\delta_x/2, \dots, (\Lambda -$

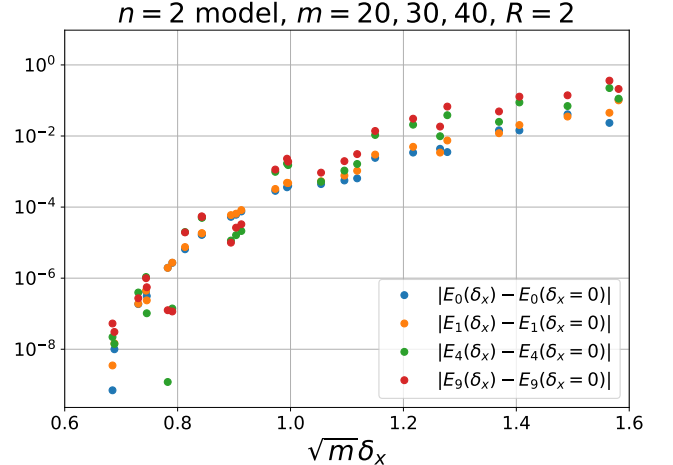


FIG. 8. For the $n = 2$ model at $R = 2$ and $m = 20, 30$, and 40 , the low-lying spectrum was calculated varying Λ (and hence $\delta_x = 2R/\Lambda$), and the difference from the values at $\delta_x = 0$ was plotted. The energy eigenvalues at $\delta_x = 0$ were estimated using sufficiently small δ_x so that the error is smaller than 10^{-10} . By using $\sqrt{m}\delta_x$ as the horizontal axis, results from different mass line up and show the same exponential decay. This means we should take $\delta_x \lesssim \frac{1}{\sqrt{m}}$ to approximate the spectrum well. Note that we plotted the absolute value $|E_\ell(\delta_x) - E_\ell(\delta_x = 0)|$ because the sign oscillates.

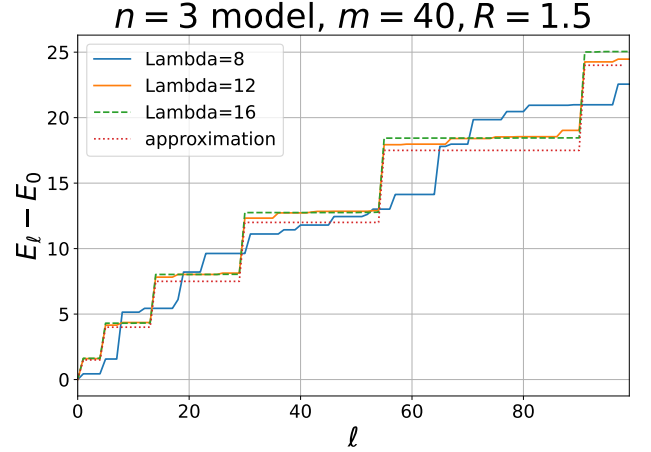


FIG. 9. $E_\ell - E_0$ ($0 \leq \ell < 100$) for the $n = 3$ model, $m = 40$, $R = 1.5$. An ‘approximation’ is obtained assuming the spectrum to be the sum of the contribution from the Laplacian on $S^3 = \text{SU}(2)$ and harmonic oscillator describing the radial coordinate, without interaction. Such an approximation is good when m is large.

$1)\delta_x/2$. The dimension of the truncated Hilbert space is Λ^2 . In the same way, we introduce $\xi \in \mathbb{C}$, so that z is transformed to $z^{(\xi)} \equiv \xi z$.

The $U(1)$ generator is

$$\hat{G} = \hat{x}\hat{p}_y - \hat{y}\hat{p}_x. \quad (39)$$

We choose $\varphi(\xi)$ in such a way that $\sum_{\xi} \varphi(\xi) |\xi\rangle$ gives the ground state of the Hamiltonian similar to (36), specifically

$$\hat{H}_{\xi} = \frac{1}{2} \hat{p}_{\xi^{(R)}}^2 + \frac{1}{2} \hat{p}_{\xi^{(I)}}^2 + \frac{m^2}{8} \left((\hat{\xi}^{(R)})^2 + (\hat{\xi}^{(I)})^2 - 1 \right)^2, \quad (40)$$

where $\xi = \xi^{(R)} + i\xi^{(I)}$, $[\hat{\xi}^{(R)}, \hat{p}_{\xi^{(R)}}] = [\hat{\xi}^{(I)}, \hat{p}_{\xi^{(I)}}] = i$, with $m = 40$, $R = 2$ and $\delta_x = 2R/\Lambda = 4/\Lambda$. We truncate $\xi^{(R)}$ and $\xi^{(I)}$ such that they take the values $\pm\delta_x/2, \pm 3\delta_x/2, \dots, (\Lambda-1)\delta_x/2$. Then, we can obtain $\sum_{\xi} \varphi(\xi) |\xi\rangle$ and $|z\rangle_{\text{proj}}$ numerically for a given $|z\rangle$. As a concrete test case, we took Λ to be even, and take $x = \frac{\delta_x}{2} (\frac{\Lambda}{2} - 1) = 1 - \frac{2}{\Lambda}$ and $y = 0$. The result is shown in Fig. 10. We can see that, as Λ increases, $\langle z |_{\text{proj}} \hat{G}^2 | z \rangle_{\text{proj}}$ quickly approaches zero.

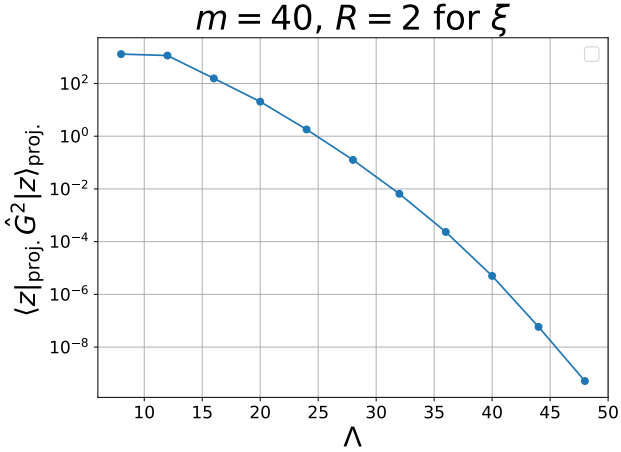


FIG. 10. $\langle z |_{\text{proj}} \hat{G}^2 | z \rangle_{\text{proj}}$, described in the text for $\Lambda = 8, 12, \dots, 48$.

The projection protocol converges exponentially with truncation level. As a result, the achievable accuracy $\Lambda = 48$ far exceeds what would be measurable on current noisy quantum hardware. This rigorous classical verification ensures the protocol will work correctly when implemented on quantum hardware at larger scales. For the complete $SU(N)$ projection, the same principles apply with additional complexity from the larger group structure. The $U(1)$ case captures the essential physics of truncation effects and validates the Haar averaging mechanism.

As discussed in Appendix C, we can simplify the setup further for $U(1)$ and \mathbb{Z}_N theories, because we do not have to introduce the scalar to describe the Hilbert space in a simple manner. Refs. [37, 38] considered the singlet projection in these cases. What is new in our protocol is that essentially the same method can be applied to non-Abelian gauge theories, and this is a reflection of the universal structure of the orbifold lattice.

D. Numerical test for Trotter decomposition

In Supplementary Material S3, the simulation cost for Hamiltonian time evolution via Trotter decomposition is estimated using standard operator-norm bounds on the error. While rigorous, this approach is conservative: the operator norm $\|\hat{H}\|$ increases with the truncation level Λ , potentially suggesting that higher cutoffs worsen simulation efficiency. However, our interest lies in *low-energy physics* — the relevant energy scales are independent of Λ , and we evolve only linear combinations of low-energy modes. In this regime, the Trotter step size should be determined by *physical* energy scales — the lattice spacing, gauge coupling, and in our setup, the scalar mass m that sets the effective cutoff — rather than by the formal UV cutoff Λ .

For the $n = 1$ model, we studied the fidelity $|\langle \psi(t)_{\text{exact}} | \psi(t)_{\text{Trotter}} \rangle|^2$; see Fig. 11, Fig. 12, and Fig. 13. From Fig. 11, we can see that the divergence of the largest energy eigenvalue as $\Lambda \rightarrow \infty$ does not affect the necessary Trotter step size for low-energy modes, as expected. On the other hand, the energy of the low-lying modes increases with m , and hence, we have to use a smaller Trotter step for larger m . In Fig. 12, we can see that the error remains approximately the same when $m\Delta t$ is fixed. Fig. 13 shows that the same step size can be used for the first few low-lying modes; this is expected because the energy is dominated by the scalar part, which is common for all low-lying modes.

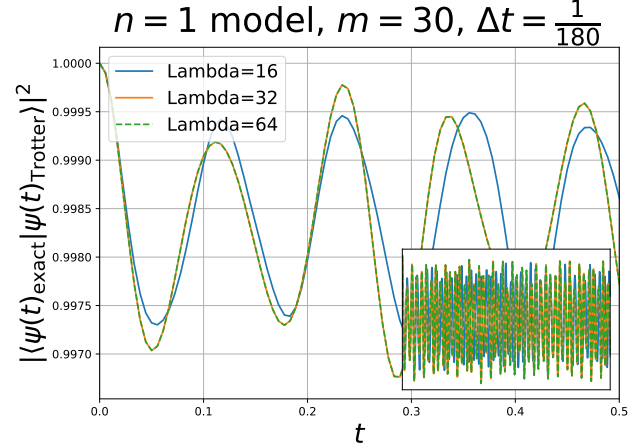


FIG. 11. Fidelity $|\langle \psi(t)_{\text{exact}} | \psi(t)_{\text{Trotter}} \rangle|^2$, $n = 1$, mass $m = 30$, step size $\Delta t = \frac{1}{180}$. We took the initial state to be the ground state of the truncated Hamiltonian. The results from $\Lambda = 32$ and $\Lambda = 64$ are indistinguishable. The inset is a plot from $t = 0$ to $t = 5$.

These results confirm the expectation stated at the beginning of this subsection: Trotter step sizes are governed by physical energy scales, not by the formal UV cutoff, ensuring that simulation efficiency is maintained even as Λ increases to improve truncation accuracy.

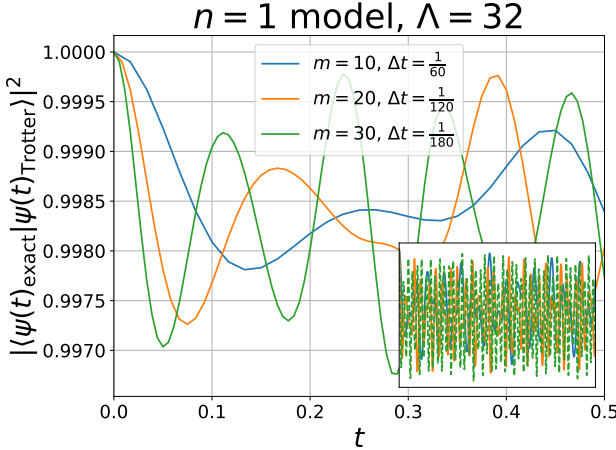


FIG. 12. Fidelity $|\langle\psi(t)_{\text{exact}}|\psi(t)_{\text{Trotter}}\rangle|^2$, $n = 1$, mass $\Lambda = 32$, and $m\Delta t = \frac{1}{6}$. We took the initial state to be the ground state of the truncated Hamiltonian. We can see that, when $m\Delta t$ is fixed, fidelity does not change with m (note the scale, the fidelity always stays very close to 1). Note that the ground state energy E_0 is proportional to m up to the truncation errors. The inset is a plot from $t = 0$ to $t = 5$.

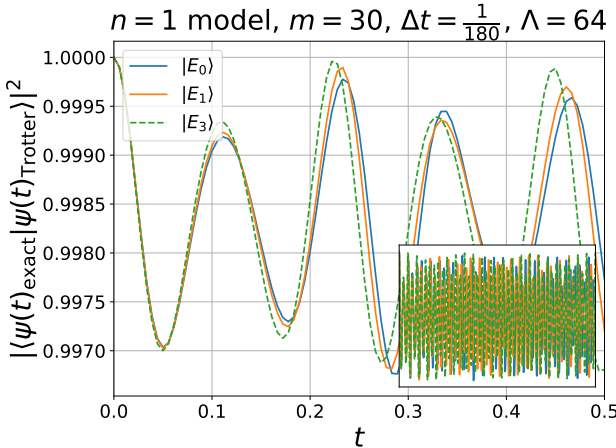


FIG. 13. Fidelity $|\langle\psi(t)_{\text{exact}}|\psi(t)_{\text{Trotter}}\rangle|^2$, $n = 1$, mass $m = 30$, truncation level $\Lambda = 64$, step size $\Delta t = \frac{1}{180}$. We took the initial state to be the ground state $|E_0\rangle$, the first excited mode $|E_1\rangle$, and the third excited mode $|E_3\rangle$. The inset is a plot from $t = 0$ to $t = 5$.

VI. RESOURCE ESTIMATES

A. Resource scaling

Building on the orbifold lattice circuits of refs. [20–23], we now provided a complete framework for gauge symmetry treatment in quantum simulation: singlet projection protocol, universal principles for choosing singlet and non-singlet formulations, and convergence

validation. Our framework enables concrete resource estimates — qubit counts, gate counts, circuit depths, and compilation costs — for Yang-Mills theory and QCD on fault-tolerant quantum computers.

Qubit counting: Assigning Q qubits for each boson, each link variable requires $2N^2Q$ qubits. For $(d + 1)$ -dimensional Yang-Mills theory on V lattice points, there are dV links, and hence, $2dN^2VQ$ qubits are needed.

For $\text{SU}(2)$, this number can be cut down to $4Q$ per boson using the embedding into \mathbb{R}^4 . For two spatial dimensions and $Q = 4$ (which corresponds to $\Lambda = 2^Q = 16$, which is promising based on the spectrum shown in Fig. 9), we need $32V$ qubits, which is 512 for a 4^2 lattice and 3200 for a 10^2 lattice. For three spatial dimensions and $Q = 4$, we need 48V qubits, which is 3072 qubits for a 4^3 lattice and 48000 qubits for a 10^3 lattice.

When Creutz [39] performed the first lattice simulation of the $\text{SU}(2)$ Yang-Mills theory that motivated many followers, he used very small lattice sizes 4^4 to 10^4 which resulted in large systematic errors which one could overcome only later. For quantum computing, if a fault-tolerant digital quantum computer with a few thousands of logical qubits becomes available, it will provide a much more solid basis and, therefore, should create even more excitement. Major quantum computer companies expect to produce machines with $O(10^4)$ logical qubits in the mid-2030s, which would allow for physics-wise relevant simulations in 3+1 dimensions, which is only about 10 years from the present.

This qubit counting does not change significantly even if the singlet-projection protocol introduced in Sec. III is used. It would be reasonable to assign the same Q to $|\xi_{\vec{n}}\rangle$ and $|Z_{j,\vec{n}}\rangle$, though it is possible to use finer mesh for ξ . Because gauge transformation is defined locally, we can perform the $\text{SU}(N)$ -averaging either simultaneously over the entire lattice, or one-by-one at each lattice point. (Of course, it is possible to perform averaging simultaneously at more than one, but not all, lattice point.) For the former approach, we need $2N^2VQ$ qubits to describe $|\xi_{\vec{n}}\rangle$ for all points \vec{n} . For the latter, we can use the same set of $|\xi\rangle$ at each time, and hence, we need to add only $2N^2Q$ qubits. Either way, this is at most the same order as the qubit requirement for the complex link fields (total $2dN^2VQ$ for d spatial dimensions). The same argument holds when we use anchilla states $\{|Z\rangle_2\}$, too.

Practically, we would not need the projection over the entire lattice; when we act a local non-singlet operator to a gauge-invariant state, we need only a local projection procedure to restore the gauge invariance.

Gate complexity: For the Hamiltonian time evolution, the simulation cost scales polynomially with Q . If we do not explicitly remove the $\text{U}(1)$ part (which is not an issue for Yang-Mills theory because $\text{U}(1)$ and $\text{SU}(N)$ sectors decouple), each Trotter step requires $O(N^2Q^2V)$ gates for Fourier transforms and $\mathcal{O}(N^4Q^4V)$ gates for quartic interactions, giving a total gate count per step of

$\mathcal{O}(N^4Q^4V)$. Circuit depth scales as $\mathcal{O}(N^4Q^4)$ when parallelization is optimized. For evolution time t with target accuracy ϵ , the number of steps in the second-order Trotterization is bounded by $\mathcal{O}(t^{3/2}E^{3/2}/\epsilon^{1/2})$ where E is the characteristic energy scale (which is not the truncation level); see Supplementary Material S3.

The addition of projections to the circuit does not affect this scaling if we avoid excessive, unnecessary use of the projections. The cost for the post-selection in the projection can be significant, and if we perform projection to the entire lattice, exponential increase of the post-selection cost looks inevitable. To tame the cost for the projection, what we should keep in mind are:

- We should use non-singlet description when possible. (Sec. IV)
- Perform singlet-projection only to a small fraction of the space, and do not repeat it too many times.

From the results in Sec. IV, we see that complications may arise only when non-singlet operators acts on a non-singlet state; therefore, we should perform the singlet projection only for such a case, in a small fraction of the lattice where such complications can arise. The use of non-singlet initial condition and singlet operators, avoiding any post-selection where possible, seems to be the optimal strategy.

Circuit design: Our simulation protocols are simple enough so that the quantum circuits can be designed mostly by hand [21]. The only part that requires a compiler is the explicit construction of one-qubit rotations from one-qubit gates, whose cost is negligible. (Of course, further optimization could be achieved by using a compiler.) This is in stark contrast with other approaches; for example, if we use a naive gauge-invariant approach, the compilation cost could increase exponentially with the total number of qubits [24].

B. Validation of convergence criteria

We validated our framework on S^n benchmark systems (Sec. V) that reproduce the essential physics of scalar mass in the orbifold formulation, including the strong-coupling limit of SU(2) theory. Key findings include:

- Truncation requirement: $\delta_x \lesssim \frac{1}{\sqrt{m}}$
- Trotter step scaling: Determined by physical energy scales such as m , not the cutoff Λ or δ_x
- Convergence rate: Rapid as Λ increases for low-energy states

For validating convergence with full gauge interactions, a classical sampling algorithm [40] can be employed — yet another advantage of non-compact variables. While such validation could provide even more precise resource estimates before fault-tolerant quantum computers arrive, it is computationally expensive and fundamentally

unnecessary: our rigorous error bounds already guarantee convergence.

VII. OUTLOOK

Our framework is complete and ready for implementation. The truncated Hamiltonian and efficient quantum circuits are given explicitly, using analytic methods. This enables us to pursue various research directions. The remaining work is optimization and experimental implementation, not algorithmic development. Specifically, immediate next steps are circuit optimization for specific architectures and specific physical process, NISQ-era demonstrations on small lattices, and classical simulation of noisy circuits. For demonstration purposes, we could try SU(2) or U(1) theory on a very small lattice — even one or two links — that is already a perfect setup to demonstrate the singlet-projection protocol; see Appendix C. Note that our protocol is straightforward and scalable given more logical qubits; even a very small-scale demonstration does not involve a simplification for the sake of demonstration that spoils the scalability.

For experimental implementation, we could consider the scattering of glueballs or hadrons. To construct a wave packet of gluons, we can take an appropriate linear combination of plaquettes, whose Pauli-string expansion can be determined analytically using only Pauli σ_z gates. Implementation and cost-estimate of such an operator are straightforward when using block encoding via LCU. Other important problems include ground-state preparation, for which the simplicity of the coordinate basis in the orbifold lattice may play a prominent role.

Concerning experiments on real quantum devices, the important point is scalability: we must study something relevant for future simulations on fault-tolerant devices and *not* study a toy model crafted for the sake of small-scale experiments. As we have seen above, $(2+1)$ -dimensional SU(2) Yang-Mills theory on a 4^2 lattice requires 512 qubits. To make quantum simulations tractable, we should also simplify the circuits. For this purpose, it is important to notice that a few terms in the orbifold lattice Hamiltonian can be dropped without affecting the infinite-mass limit [20]. By dropping a few terms, the number of gates needed for one Trotter step can be reduced, while the number of qubits needed for sufficiently precise descriptions may or may not change. The point we really want to make in this paper is that the combination of the orbifold lattice formulation, the rapid increase in quantum computer resources and the various optimization steps we and others suggest could imply that practical quantum computing for lattice gauge theory is substantially closer than one might fear.

The quantum simulation of non-Abelian gauge theories has advanced from theoretical possibility to practical readiness. Our framework provides everything needed for implementation: explicit quantum circuits with polynomial scaling, protocols for gauge-singlet projection when

desired, validated convergence criteria, and complete resource estimates. By working in an extended Hilbert space and using the orbifold lattice formulation, we avoid the exponential classical preprocessing that plagues alternative approaches. The universal principles we establish — clarifying when and why singlet and non-singlet formulations work — apply beyond our specific implementation to any quantum simulation approach. Our numerical validations demonstrate that truncation errors are controllable and that Trotter step sizes are determined by physical energy scales rather than formal cutoffs, confirming practical efficiency. For SU(2) Yang-Mills theory in 2+1 dimensions, the number of logical qubits needed for small lattices aligns with quantum computing roadmaps for the mid-2030s. For demonstration purpose, we could try SU(2) or U(1) theory on a very small lattice, even one or two links; see Appendix C for concrete qubit requirements and scalability analysis.

The path from current algorithms to future quantum advantage in gauge theory simulation is now clear and concrete. What remains is not algorithmic development, but hardware maturation and experimental optimization — the transition from if to when.

ACKNOWLEDGEMENT

We thank Masaki Tezuka for discussions and support for some computations in Sec. V. We thank Georg Bergner, Yuta Kikuchi, Lento Nagano, Shinsuke Nishigaki, Enrico Rinaldi, and Yuki Sato for discussions and comments. M. H. thanks the STFC for the support through the consolidated grant ST/Z001072/1. Sec. II and Sec. IV are largely based on materials prepared for M. H.’s talk at “Quantum Simulation of Strong Interactions (QuaSI) Workshop 1 : Theoretical Strategies for Gauge Theories” at InQubator for Quantum Simulation, the University of Washington, in April 2021. They were not presented in the main sessions due to time limitations, but discussions with the participants were certainly useful.

Appendix A: Review of Kogut-Susskind formulation

The Kogut-Susskind Hamiltonian [41] (see e.g., ref. [42] for a review) is a Hamiltonian counterpart of Wilson’s lattice action [43]. A crucial point is to introduce a lattice regularization that preserves important symmetries of the continuum theory in such a way that the radiative corrections are under control. At the lattice level, the Kogut-Susskind Hamiltonian has discrete translation (translation by a lattice unit), 90-degree rotations, parity, charge conjugation, and gauge symmetry.

1. Operators and commutation relations

To realize the lattice version of gauge symmetry, unitary link variables that correspond to $\exp(iagA_j)$ are used. Here, a and g are the lattice spacing and coupling constant, respectively. The link variable $U_{j,\vec{n}}$ lives on a link connecting a point \vec{n} and the neighboring point $\vec{n} + \hat{j}$, and the gauge transformation is defined by $U_{j,\vec{n}} \rightarrow \Omega_{\vec{n}} U_{j,\vec{n}} \Omega_{\vec{n} + \hat{j}}^{-1}$. As mentioned above, the electric field E_j is the conjugate momentum of A_j . Therefore, we want something like $[\hat{E}_{j,\vec{n}}, \hat{A}_{j',\vec{n}'}] = -i\delta_{jj'}\delta_{\vec{n}\vec{n}'}/a^3$. Note that $\delta_{\vec{n}\vec{n}'}/a^3$ is the lattice version of delta function.

Let τ_α be the generator of the group ($\alpha = 1, \dots, N^2$ for $U(N)$ and $\alpha = 1, \dots, N^2 - 1$ for $SU(N)$), which is normalized as $\text{Tr}(\tau_\alpha \tau_\beta) = \delta_{\alpha\beta}$. We write an $N \times N$ matrix E_j as $E_j = \sum_\alpha E_j^\alpha \tau_\alpha$. Then, $U_{j,\vec{n}} = \exp(iagA_{j,\vec{n}}^\alpha \tau_\alpha)$, and hence, as an analog of $[\hat{E}_{j,\vec{n}}, \hat{A}_{j',\vec{n}'}] = -i\delta_{jj'}\delta_{\vec{n}\vec{n}'}/a^3$ we can take the commutation relations

$$[\hat{E}_{j,\vec{n}}^\alpha, \hat{U}_{k,\vec{n}'}^{pq}] = a^{-2} g \delta_{jk} \delta_{\vec{n}\vec{n}'} (\tau_\alpha \hat{U}_{k,\vec{n}'}^{pq})^{pq}, \quad (\text{A1})$$

$$[\hat{E}_{j,\vec{n}}^\alpha, \hat{U}_{k,\vec{n}'}^{\dagger pq}] = -a^{-2} g \delta_{jk} \delta_{\vec{n}\vec{n}'} (\hat{U}_{k,\vec{n}'}^{\dagger pq} \tau_\alpha)^{pq}. \quad (\text{A2})$$

From the Jacobi identity, we also have

$$[\hat{E}_{j,\vec{n}}^\alpha, \hat{E}_{k,\vec{n}'}^\beta] = -ia^{-2} g \sum_\gamma f^{\alpha\beta\gamma} \delta_{jk} \delta_{\vec{n}\vec{n}'} \hat{E}_{k,\vec{n}'}^\gamma, \quad (\text{A3})$$

where $f^{\alpha\beta\gamma}$ is the structure constant:

$$[\tau_\alpha, \tau_\beta] = i \sum_\gamma f_{\alpha\beta\gamma} \tau_\gamma. \quad (\text{A4})$$

Here, we defined the electric field operator \hat{E}_j using an infinitesimal transformation acting from the left of the link variable. We can also use an infinitesimal transformation acting from the right of the link variable, but as we will see later, using only the former is enough.

We can choose the generators in such a way that

$$\sum_{\alpha=1}^{N^2} \tau_{pq}^\alpha \tau_{rs}^\alpha = \delta_{ps} \delta_{qr}, \quad \sum_{\alpha=1}^{N^2} (\tau^\alpha \tau^\alpha)_{pq} = N \delta_{pq} \quad (\text{A5})$$

are satisfied for $U(N)$ and

$$\sum_\alpha \tau_\alpha^{pq} \tau_\alpha^{rs} = \delta^{ps} \delta^{qr} - \frac{\delta^{pq} \delta^{rs}}{N},$$

$$\sum_{\alpha=1}^{N^2} (\tau^\alpha \tau^\alpha)_{pq} = \left(1 - \frac{1}{N^2}\right) N \delta_{pq} \quad (\text{A6})$$

are satisfied for $SU(N)$.

Unlike \hat{E} ’s, \hat{U} ’s commute with each other:

$$[\hat{U}, \hat{U}] = [\hat{U}, \hat{U}^\dagger] = [\hat{U}^\dagger, \hat{U}^\dagger] = 0. \quad (\text{A7})$$

2. Kogut-Susskind Hamiltonian

The Hamiltonian consists of electric and magnetic terms,

$$\hat{H} = \hat{H}_E + \hat{H}_B. \quad (\text{A8})$$

The electric part is

$$\hat{H}_E = \frac{a^3}{2} \sum_{\vec{n}} \sum_{j=1}^3 \sum_{\alpha=1}^{N^2} \left(\hat{E}_{j,\vec{n}}^{\alpha} \right)^2. \quad (\text{A9})$$

The magnetic part is

$$\hat{H}_B = \frac{1}{2ag^2} \sum_{\vec{n}} \sum_{j \neq k} \text{Tr} \left(\mathbf{1} - \hat{U}_{j,\vec{n}} \hat{U}_{k,\vec{n}+j} \hat{U}_{j,\vec{n}+k}^{\dagger} \hat{U}_{k,\vec{n}}^{\dagger} \right). \quad (\text{A10})$$

The magnetic term (plaquette) is dropped in the strong coupling limit, $g^2 \rightarrow \infty$ [44]. Note that this “strong coupling limit” is different from the continuum limit, which is obtained by scaling the coupling constant and lattice spacing to zero properly.

The ground state of this strong-coupling lattice gauge theory Hamiltonian $|g.s.\rangle$ satisfies $\hat{E}_{j,\vec{n}}^{\alpha} |g.s.\rangle = 0$ for any α, j and \vec{n} . Hence, let us use the notation $|E = 0\rangle$ to denote the ground state.

The operator $\hat{U}_{j,\vec{n}}$ is interpreted as the coordinate of the group manifold $G = \text{U}(N)$ or $\text{SU}(N)$ for the link variable on the site \vec{n} in the j -direction. The operators \hat{U} and \hat{E} are defined on the extended Hilbert space \mathcal{H}_{ext} that contains gauge non-singlet modes. A convenient basis of \mathcal{H}_{ext} is the coordinate representation,

$$\mathcal{H}_{\text{ext}} = \otimes_{j,\vec{n}} \mathcal{H}_{j,\vec{n}} \sim \otimes_{j,\vec{n}} (\oplus_{g \in G} |g\rangle_{j,\vec{n}}), \quad (\text{A11})$$

where

$$\hat{U}_{j,\vec{n}} |g\rangle_{j,\vec{n}} = g |g\rangle_{j,\vec{n}} \quad g \in G \quad (\text{A12})$$

More precisely, we will consider only the Hilbert space of square-integrable wave functions. The ground state is the constant mode,

$$\begin{aligned} |E = 0\rangle &= \otimes_{\mu,\vec{n}} |E = 0\rangle_{j,\vec{n}}, \\ |E = 0\rangle_{j,\vec{n}} &= \frac{1}{\sqrt{\text{vol}G}} \int_G dg |g\rangle_{j,\vec{n}}. \end{aligned} \quad (\text{A13})$$

Namely, the wave function $\langle g|E = 0\rangle$ is constant.

Let $G_{\vec{n}}$ be the group G living on a point \vec{n} , and $\mathcal{G} = \prod_{\vec{n}} G_{\vec{n}}$ be the group of all local gauge transformations. Gauge transformation by $\hat{\Omega} = \otimes_{\vec{n}} \hat{\Omega}_{\vec{n}}$ is defined by

$$\hat{\Omega} \left(\otimes_{j,\vec{n}} |g\rangle_{j,\vec{n}} \right) = \otimes_{j,\vec{n}} \left(\hat{\Omega}_{\vec{n}} |g\rangle_{j,\vec{n}} \right) = \otimes_{j,\vec{n}} \left| \Omega_{\vec{n}} g \Omega_{\vec{n}+j}^{-1} \right\rangle_{j,\vec{n}}. \quad (\text{A14})$$

Note that the strong-coupling ground state is gauge-invariant:

$$\hat{\Omega} |E = 0\rangle = |E = 0\rangle. \quad (\text{A15})$$

We can define the projection operator to the gauge-invariant Hilbert space \mathcal{H}_{inv} as

$$\hat{\mathcal{P}} = \frac{1}{\text{Vol}\mathcal{G}} \int_{\mathcal{G}} d\Omega \hat{\Omega}, \quad (\text{A16})$$

where the integral is taken by using the Haar measure. By using this projection operator, the canonical partition function at temperature T can be written in two ways as [32]

$$Z(T) = \text{Tr}_{\mathcal{H}_{\text{inv}}} \left(e^{-\hat{H}/T} \right) \quad (\text{A17})$$

and

$$Z(T) = \text{Tr}_{\mathcal{H}_{\text{ext}}} \left(\hat{\mathcal{P}} e^{-\hat{H}/T} \right). \quad (\text{A18})$$

The latter expression is directly related to the path-integral formalism with gauge field A_t , as shown in Supplementary Material S2. The insertion of the projector $\hat{\mathcal{P}}$ means we should identify the states connected by a gauge transformation.

3. Strings and interactions

Below, we consider $\text{U}(N)$ gauge theory, because the expressions are slightly simpler than for the case of $\text{SU}(N)$.

A closed string is created by the Wilson loop

$$\hat{W} = \text{Tr}(\hat{U}_{j,\vec{n}} \hat{U}_{k,\vec{n}+j} \cdots), \quad (\text{A19})$$

where the product of \hat{U} 's in the trace is taken along a closed path. This is a counterpart of (19) in the Kogut-Susskind formulation. Suppose the loop does not have self-intersection, in the sense that no link appears more than once. Then, $\hat{W} |E = 0\rangle$ is an energy eigenstate, and the energy is proportional to the length La (equivalently, the number of links in the Wilson loop L), as we can see as follows. First, because $|E = 0\rangle$ is annihilated by \hat{E} , we have

$$\begin{aligned} &\sum_{\alpha} \left(\hat{E}_{j,\vec{n}}^{\alpha} \right)^2 \hat{W} |E = 0\rangle \\ &= \sum_{\alpha} \left[\hat{E}_{j,\vec{n}}^{\alpha}, \left[\hat{E}_{j,\vec{n}}^{\alpha}, \hat{W} \right] \right] |E = 0\rangle. \end{aligned} \quad (\text{A20})$$

$\hat{E}_{j,\vec{n}}^{\alpha}$ commutes with \hat{W} unless the latter contains $\hat{U}_{j,\vec{n}}$ or $\hat{U}_{j,\vec{n}}^{\dagger}$. When $\hat{U}_{j,\vec{n}}$ is contained,

$$\begin{aligned} &\sum_{\alpha} \left[\hat{E}_{j,\vec{n}}^{\alpha}, \left[\hat{E}_{j,\vec{n}}^{\alpha}, \hat{W} \right] \right] \\ &= \sum_{\alpha} \text{Tr} \left(\left[\hat{E}_{j,\vec{n}}^{\alpha}, \left[\hat{E}_{j,\vec{n}}^{\alpha}, \hat{U}_{j,\hat{n}} \right] \right] \hat{U}_{k,\hat{n}+j} \cdots \right) \\ &= (a^{-2} g)^2 \sum_{\alpha} \text{Tr} \left(\tau^{\alpha} \tau^{\alpha} \hat{U}_{j,\hat{n}} \hat{U}_{k,\hat{n}+j} \cdots \right) \\ &= a^{-4} g^2 N \text{Tr} \left(\hat{U}_{j,\hat{n}} \hat{U}_{k,\hat{n}+j} \cdots \right) \\ &= a^{-4} g^2 N \hat{W}. \end{aligned} \quad (\text{A21})$$

The same holds when $\hat{U}_{j,\hat{n}}^\dagger$ is in the loop. Therefore,

$$\hat{H}_E \hat{W} |0\rangle = L \cdot \frac{g^2 N}{2a} \hat{W} |0\rangle. \quad (\text{A22})$$

The same holds for any multi-string state, including closed or open strings, as long as there is no intersection. Note that $g^2 N$ is the 't Hooft coupling, which is fixed in the 't Hooft large- N limit. The interpretation is clear: the energy of a string is its length La times the string tension $\frac{g^2 N}{2a^2}$.

Next, let us consider the case with intersections. Suppose a link $\hat{U}_{j,\vec{n}}$ appears twice in the loop, while all other links appear only once. (Generalization to generic situation is straightforward.) Let us write such a loop as $\text{Tr}(\hat{V}_1 \hat{U}_{j,\vec{n}} \hat{V}_2 \hat{U}_{j,\vec{n}})$. Then,

$$\begin{aligned} & \sum_{\alpha} \left[\hat{E}_{j,\vec{n}}^{\alpha}, \left[\hat{E}_{j,\vec{n}}^{\alpha}, \text{Tr}(\hat{V}_1 \hat{U}_{j,\vec{n}} \hat{V}_2 \hat{U}_{j,\vec{n}}) \right] \right] \\ &= 2a^{-4} g^2 N \text{Tr}(\hat{V}_1 \hat{U}_{j,\vec{n}} \hat{V}_2 \hat{U}_{j,\vec{n}}) \\ &+ 2 \sum_{\alpha} \text{Tr}(\hat{V}_1 [\hat{E}_{j,\vec{n}}^{\alpha}, \hat{U}_{j,\vec{n}}] \hat{V}_2 [\hat{E}_{j,\vec{n}}^{\alpha}, \hat{U}_{j,\vec{n}}]) \\ &= 2a^{-4} g^2 N \text{Tr}(\hat{V}_1 \hat{U}_{j,\vec{n}} \hat{V}_2 \hat{U}_{j,\vec{n}}) \\ &+ 2a^{-4} g^2 \sum_{\alpha} \text{Tr}(\hat{V}_1 \tau^{\alpha} \hat{U}_{j,\vec{n}} \hat{V}_2 \tau^{\alpha} \hat{U}_{j,\vec{n}}) \\ &= 2a^{-4} g^2 N \text{Tr}(\hat{V}_1 \hat{U}_{j,\vec{n}} \hat{V}_2 \hat{U}_{j,\vec{n}}) \\ &+ 2a^{-4} g^2 \text{Tr}(\hat{V}_1 \hat{U}_{j,\vec{n}}) \text{Tr}(\hat{V}_2 \hat{U}_{j,\vec{n}}). \end{aligned} \quad (\text{A23})$$

Therefore,

$$\begin{aligned} & \hat{H}_E \left(\text{Tr}(\hat{V}_1 \hat{U}_{j,\vec{n}} \hat{V}_2 \hat{U}_{j,\vec{n}}) |E=0\rangle \right) \\ &= L \cdot \frac{g^2 N}{2a} \text{Tr}(\hat{V}_1 \hat{U}_{j,\vec{n}} \hat{V}_2 \hat{U}_{j,\vec{n}}) |E=0\rangle \\ &+ \frac{g^2}{a} \text{Tr}(\hat{V}_1 \hat{U}_{j,\vec{n}}) \text{Tr}(\hat{V}_2 \hat{U}_{j,\vec{n}}) |E=0\rangle. \end{aligned} \quad (\text{A24})$$

The second term can be understood as the splitting of a string into two strings. Note that the second term is suppressed by a factor of $1/N$ compared to the first term. Similarly, two strings can be joined at an intersection to form one string,

$$\begin{aligned} & \hat{H}_E \left(\text{Tr}(\hat{V}_1 \hat{U}_{j,\vec{n}}) \text{Tr}(\hat{V}_2 \hat{U}_{j,\vec{n}}) |E=0\rangle \right) \\ &= L \cdot \frac{g^2 N}{2a} \text{Tr}(\hat{V}_1 \hat{U}_{j,\vec{n}}) \text{Tr}(\hat{V}_2 \hat{U}_{j,\vec{n}}) |E=0\rangle \\ &+ \frac{g^2}{a} \text{Tr}(\hat{V}_1 \hat{U}_{j,\vec{n}} \hat{V}_2 \hat{U}_{j,\vec{n}}) |E=0\rangle. \end{aligned} \quad (\text{A25})$$

In general, such splitting and joining can take place at any intersection.

We can also use the counterpart of the non-singlet loop (20), which is defined by

$$\hat{W}^{(\text{non-singlet})} \equiv N^l \hat{U}_{j_1, \vec{x}; a_1 a_2} \hat{U}_{j_2, \vec{x} + \hat{j}_1; a_2 a_3} \cdots \hat{U}_{j_l, \vec{x} - \hat{j}_l; a_l a_1}. \quad (\text{A26})$$

Straightforward computations show that exactly the same results hold: for non-intersecting strings, \hat{H}_E counts the number of links; when strings intersect, joining/splitting takes place; and numerical factors are also the same.

One difference, which may look troublesome at first glance, is that $\hat{U}_{j,\vec{n}}^{ab} \hat{U}_{j,\vec{n}}^{\dagger bc}$ is not δ^{ac} if a sum over b is not taken. In general, $\hat{W}^{(\text{non-singlet})}$ with and without whiskers (Figure 2) becomes identical after the projection to the singlet, and hence, their difference is a redundant state that is in $\text{Ker}(\hat{\mathcal{P}})$. When the expectation value is taken using gauge-invariant states like the ground state, whiskers becomes 1.

Note that, even if the initial state is non-singlet, singlet states can also emerge through the interaction between plaquettes and strings in the initial state, as we can see in Figure 14.

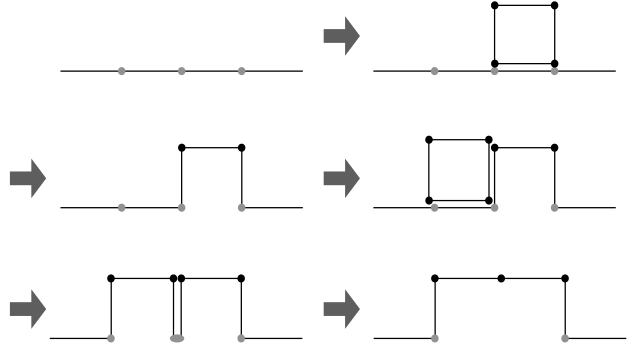


FIG. 14. Interaction between non-singlet string and plaquettes in the Kogut-Susskind Hamiltonian, which are, by construction, singlets. Straight lines are link variables (string bits), and black and grey circles stand for indices which are summed (from 1 to N) and not summed.

In the above, we used the electric field defined from the infinitesimal transformation acting from the left of the link variable. We could also use the one acting from the right, and the result is the same anyway; see Supplementary Material S6.

Appendix B: Review of orbifold lattice formulation

In this section, we review the orbifold lattice Hamiltonian approach for quantum simulations of gauge theory [19–23]. For concreteness, we consider 3 + 1-d pure $SU(N)$ Yang-Mills theory, formulated on the extended Hilbert space.

1. Operators and commutation relations

The orbifold lattice Hamiltonian [19, 20, 45] can be written in terms of the complex link variables $Z_{j,\vec{n}}$ ($j = 1, 2, 3$), and their canonical conjugates $P_{j,\vec{n}}$.

Note that $\bar{Z}_{j,\vec{n}}$ and $\bar{P}_{j,\vec{n}}$ stand for Hermitian conjugates of $N \times N$ matrices, i.e.,

$$\bar{Z}_{j,\vec{n};ab} = (Z_{j,\vec{n};ba})^*, \quad \bar{P}_{j,\vec{n};ab} = (P_{j,\vec{n};ba})^*. \quad (\text{B1})$$

We do not use dagger \dagger because we save it for conjugate operators acting on the Hilbert space. For the operators this implies

$$\hat{Z}_{j,\vec{n};ab} = \left(\hat{Z}_{j,\vec{n};ba} \right)^\dagger, \quad \hat{P}_{j,\vec{n};ab} = \left(\hat{P}_{j,\vec{n};ba} \right)^\dagger, \quad (\text{B2})$$

The canonical commutation relation is

$$[\hat{Z}_{j,\vec{n};ab}, \hat{P}_{k,\vec{n}';cd}] = \left[\hat{Z}_{j,\vec{n};ab}, \left(\hat{P}_{k,\vec{n}';dc} \right)^\dagger \right] = i\delta_{jk}\delta_{\vec{n}\vec{n}'}\delta_{ad}\delta_{bc}. \quad (\text{B3})$$

In case one prefers real variables, Z can be separated into real and imaginary parts x and y ,

$$\hat{Z}_{j,\vec{n};ab} = \frac{\hat{x}_{j,\vec{n};ab} + i\hat{y}_{j,\vec{n};ab}}{\sqrt{2}}, \quad (\text{B4})$$

and their conjugate momenta $p^{(x)}$ and $p^{(y)}$,

$$\hat{P}_{j,\vec{n};ab} = \frac{\hat{p}_{j,\vec{n};ab}^{(x)} + i\hat{p}_{j,\vec{n};ab}^{(y)}}{\sqrt{2}}, \quad (\text{B5})$$

that satisfy

$$[\hat{x}_{j,\vec{n};ab}, \hat{p}_{k,\vec{n}';cd}^{(x)}] = [\hat{y}_{j,\vec{n};ab}, \hat{p}_{k,\vec{n}';cd}^{(y)}] = i\delta_{jk}\delta_{\vec{n}\vec{n}'}\delta_{ad}\delta_{bc}, \quad (\text{B6})$$

while other commutators vanish. The orbifold lattice Hamiltonian is designed so that Yang-Mills theory coupled to scalars is obtained when the complex link variable Z is expanded about an appropriate background.

The complex link variable Z can be interpreted as a product of a positive-definite Hermitian site variable W and a unitary link variable U as [46]

$$Z_{j,\vec{n}} = \sqrt{\frac{a}{2g^2}} W_{j,\vec{n}} U_{j,\vec{n}}. \quad (\text{B7})$$

They describe an adjoint scalar field ϕ_j and gauge field A_j , respectively, as $W_{j,\vec{n}} = \exp(ag\phi_{j,\vec{n}})$ and $U_{j,\vec{n}} = \exp(iagA_{j,\vec{n}})$. Intuitively, W and U are the polar coordinates, with the radial coordinate W and angular coordinate U , while the Z are the Cartesian coordinates. The key observation [19, 20] is that quantization is straightforward in Cartesian coordinates. Indeed, we can use $2N^2$ bosons \hat{x}_a and \hat{p}_a ($a = 1, \dots, 2N^2$) that satisfy the canonical commutation relation $[\hat{x}_a, \hat{p}_b] = \delta_{ab}$ to describe the real and imaginary parts of each link variable $Z_{j,\vec{n}}$. This simple fact resolves technical difficulties associated with the Kogut-Susskind Hamiltonian formulation.

2. Orbifold lattice Hamiltonian

The orbifold lattice Hamiltonian has been studied as a convenient tool to achieve exponential speedup in quantum simulations of Yang-Mills theory and QCD. The orbifold lattice Hamiltonian for pure Yang-Mills theory is [19, 20, 45]

$$\begin{aligned} \hat{H} = & \sum_{\vec{n}} \text{Tr} \left(\sum_{j=1}^3 \hat{P}_{j,\vec{n}} \hat{P}_{j,\vec{n}} \right. \\ & + \frac{g^2}{2a^3} \left| \sum_{j=1}^3 \left(\hat{Z}_{j,\vec{n}} \hat{Z}_{j,\vec{n}} - \hat{Z}_{j,\vec{n}-\hat{j}} \hat{Z}_{j,\vec{n}-\hat{j}} \right) \right|^2 \\ & + \frac{2g^2}{a^3} \sum_{j < k} \left| \hat{Z}_{j,\vec{n}} \hat{Z}_{k,\vec{n}+\hat{j}} - \hat{Z}_{k,\vec{n}} \hat{Z}_{j,\vec{n}+\hat{k}} \right|^2 \left. \right) \\ & + \hat{H}^{(\text{mass})}, \end{aligned} \quad (\text{B8})$$

where $\hat{H}^{(\text{mass})}$ is chosen appropriately depending on the details of the strategy. Ref. [22] used

$$\begin{aligned} \hat{H}^{(\text{mass})} \equiv & \frac{m^2 g^2}{2a} \sum_{\vec{n}} \sum_{j=1}^3 \text{Tr} \left| \hat{Z}_{j,\vec{n}} \hat{Z}_{j,\vec{n}} - \frac{a}{2g^2} \cdot \mathbf{1}_N \right|^2 \\ & + \frac{m_{\text{U}(1)}^2 a}{2g^2} \sum_{\vec{n}} \sum_{j=1}^3 \left| \left(\frac{a}{2g^2} \right)^{-N/2} \det(\hat{Z}_{j,\vec{n}}) - 1 \right|^2. \end{aligned} \quad (\text{B9})$$

With this choice, in the large-mass limit $m^2, m_{\text{U}(1)}^2 \rightarrow \infty$, the complex links reduce to unitary links as $Z_{j,\vec{n}} = \sqrt{\frac{a}{2g^2}} W_{j,\vec{n}} U_{j,\vec{n}} \rightarrow \sqrt{\frac{a}{2g^2}} U_{j,\vec{n}}$, $\det U_{j,\vec{n}}$ becomes 1, and the orbifold lattice Hamiltonian reduces to the $\text{SU}(N)$ Kogut-Susskind Hamiltonian. Away from the Kogut-Susskind limit, the orbifold lattice Hamiltonian describes Yang-Mills theory coupled to heavy scalars that do not affect low-energy physics. (Note that the last term in (B9) is not important, because the $\text{U}(1)$ part decouples from the $\text{SU}(N)$ part.)

The orbifold lattice Hamiltonian and the commutation relation are invariant under the local $\text{U}(N)$ transformation

$$\hat{Z}_{j,\vec{n}}, \hat{P}_{j,\vec{n}} \rightarrow \Omega_{\vec{n}}^{-1} \hat{Z}_{j,\vec{n}} \Omega_{\vec{n}+\hat{j}}, \Omega_{\vec{n}}^{-1} \hat{P}_{j,\vec{n}} \Omega_{\vec{n}+\hat{j}}, \quad (\text{B10})$$

where $\Omega_{\vec{n}}$ is an $N \times N$ unitary matrix. We can gauge only $\text{SU}(N)$ [20]. Note that $W_{j,\vec{n}}$ and $U_{j,\vec{n}}$ transform as an adjoint scalar on a site and unitary link variables, respectively [46] :

$$\hat{W}_{j,\vec{n}}, \hat{U}_{j,\vec{n}} \rightarrow \Omega_{\vec{n}}^{-1} \hat{W}_{j,\vec{n}} \Omega_{\vec{n}}, \Omega_{\vec{n}}^{-1} \hat{U}_{j,\vec{n}} \Omega_{\vec{n}+\hat{j}}. \quad (\text{B11})$$

3. Strings and interactions

We can use singlet and non-singlet version of the Wilson loops $\hat{W}_{\text{closed}}^{(\text{singlet})}$ and $\hat{W}_{\text{closed}}^{(\text{non-singlet})}$ defined in (19) and

(20), respectively. They describe QCD strings coupled to scalars.

It is easy to see that joining and splitting of strings takes place as in the Kogut-Susskind formulation. Indeed, similar to (A23) for the Kogut-Susskind formulation, there are splitting processes such as

$$\begin{aligned} \sum_{a,b} \left[\hat{P}_{j,\vec{n},ab}, \left[\hat{P}_{j,\vec{n},ba}^\alpha, \text{Tr}(\hat{V}_1 \hat{Z}_{j,\vec{n}} \hat{V}_2 \hat{Z}_{j,\vec{n}}) \right] \right] \\ = - \left(\text{Tr} \hat{V}_1 \right) \left(\text{Tr} \hat{V}_2 \right). \end{aligned} \quad (\text{B12})$$

Still, some care is needed to see a precise correspondence to the Kogut-Susskind formulation, as we see below.

Unlike the electric field operator \hat{E} in the Kogut-Susskind formulation, the momentum operators \hat{P} and $\hat{\bar{P}}$ annihilates links, or string bits, \hat{Z} and $\hat{\bar{Z}}$. Therefore, the kinetic term $\text{Tr}(\hat{P}\hat{\bar{P}})$ itself does not count the number of links. It has to be combined with the mass term \hat{H}_{mass} , so that links are close to unitary in the low-energy states. The same is true for the ‘whiskers’ (Figure 2). When the mass is large and scalars are suppressed, loop operators with and without whiskers are indistinguishable as long as they act on the low-energy states.

4. Truncated Hamiltonian in terms of Pauli strings

Unlike in the naive Kogut-Susskind approach, the orbifold lattice Hamiltonian can easily be truncated to finite dimension and be expressed in terms of Pauli strings [19, 20].

Link variables in the orbifold lattice can be described like the standard bosons \hat{x}_a and \hat{p}_a ($a = 1, 2, \dots, 2N^2 n_\ell$), where n_ℓ is the number of links (for the periodic boundary condition, the number of lattice sites times the spatial dimensions). The extended Hilbert space can be expressed using either the coordinate basis or the momentum basis. The coordinate basis is defined as

$$\mathcal{H}_{\text{ext}} = \otimes_a \mathcal{H}_a, \quad \mathcal{H}_a = \text{Span}\{|x_a\rangle |x_a \in \mathbb{R}\}, \quad (\text{B13})$$

where

$$\hat{x}_a |x_a\rangle = x_a |x_a\rangle. \quad (\text{B14})$$

The momentum basis is defined using the momentum eigenstate,

$$\hat{p}_a |p_a\rangle = p_a |p_a\rangle. \quad (\text{B15})$$

The coordinate basis and momentum basis are related by Fourier transform.

To put this Hilbert space on a digital quantum computer, we can introduce a cutoff for each boson coordinate x_a . We allocate Q qubits to each boson. Each x_a may assume $\Lambda = 2^Q$ distinct values. For practical purposes, it proves advantageous to implement periodic boundary

conditions $x + 2R \sim x$. In this framework, a convenient choice is

$$\delta_x = \frac{2R}{\Lambda} \quad (\text{B16})$$

and

$$\hat{x}_a = -\delta_x \cdot \left(\frac{\sigma_{z,1}}{2} + 2 \cdot \frac{\sigma_{z,2}}{2} + \dots + 2^{Q-1} \cdot \frac{\sigma_{z,Q}}{2} \right). \quad (\text{B17})$$

Here, $\sigma_{z,j}$ represents the Pauli σ_z operator acting on the j -th qubit assigned to the a -th boson, and Pauli σ_z operators defined as

$$\sigma_z \equiv |0\rangle\langle 0| - |1\rangle\langle 1|. \quad (\text{B18})$$

Consequently, \hat{x}_a takes values $\pm \frac{\delta_x}{2}, \pm \frac{3\delta_x}{2}, \dots, \pm \frac{(\Lambda-1)\delta_x}{2}$. In the same way, in the momentum basis, we have

$$\hat{p}_a = -\delta_p \cdot \left(\frac{\sigma_{z,1}}{2} + 2 \cdot \frac{\sigma_{z,2}}{2} + \dots + 2^{Q-1} \cdot \frac{\sigma_{z,Q}}{2} \right), \quad (\text{B19})$$

where

$$\delta_p = \frac{\pi}{R}. \quad (\text{B20})$$

Note that the coordinate basis and momentum basis are related, at the discretized level, by a Fourier transform, which can be performed efficiently on a digital quantum computer. We use \hat{F} to denote the Fourier transform from the coordinate basis to the momentum basis. This is a product of Fourier transforms for each boson, which are denoted by \hat{F}_a : $\hat{F} = \prod_a \hat{F}_a$.

Numerous polynomial couplings exist in the form $\hat{x}_a \otimes \hat{x}_b \otimes \dots$. In the coordinate basis, each \hat{x} comprises a weighted sum of $\sigma_{z,1}, \dots, \sigma_{z,Q}$. Therefore, couplings in the orbifold lattice Hamiltonian are written as weighted sums of Pauli strings consisting of Pauli σ_z 's.

Appendix C: Potential near-term demonstrations on quantum devices

Though our simulation protocols are theoretically justified to scale well, it is always good to have experimental demonstrations on quantum devices. In the near future, we would want to focus on the minimal setups. The smallest possible example would be the single-site lattice — whose large- N version is known as the Eguchi-Kawai model [47] and provides us with a practically useful tool to study lattice gauge theory via large- N volume reduction [47, 48] — with d links (that corresponds to the spatial dimension d) and $SU(2)$ gauge group. The value of d can be 1 or 2. While $d = 2$ is needed for nontrivial interactions, $d = 1$ is enough for a demonstration purpose.

As we saw in Sec. V, we can represent each link and ancilla state $|\xi\rangle$ using four bosons, and $Q = 4$ ($\Lambda = 2^Q =$

16) is reasonably good for low-energy spectrum. If we do not use the OAA to increase the success rate of the post selection for the singlet projection, we need only one ancilla state $|Z\rangle_2$, which requires four boson; hence we need $4(d+2)Q = 16(d+2)$ qubits. Taking $d = 1$ or 2, we get 48 or 64 qubits. We can also try SU(2) Hermitian d -matrix model (see e.g., [49]), where dynamical variables are SU(2) Hermitian matrices consisting of 3 bosons; then we need $3d$ bosons for dynamical degrees of freedom, 3 bosons for the ancilla state analogous to $|Z\rangle_2$, and 4 bosons for ξ , and hence total $(3d+7)Q$ qubits. Taking $Q = 4$ and $d = 1$ or 2, we get 40 or 52 qubits.

These numbers are promising but one would want something even smaller to have demonstrations as soon as possible. For that purpose, projection for n_ℓ links of U(1) theory embedded into \mathbb{R}^2 , described in Supplementary Material S5B, may be useful. Having $|Z\rangle_1$, $|Z\rangle_2$, and ξ , we need only $2(n_\ell + 2)$ bosons ($2n_\ell$ for $|Z\rangle_1$, two for $|Z\rangle_2$ and two for ξ), and $2(n_\ell + 2)Q$ qubits.

For U(1) and \mathbb{Z}_n theories, we can simplify the setup further. The key point is that we do not have to introduce the scalar to truncate U(1) efficiently, because it is a compactification of \mathbb{R} , and \mathbb{Z}_n is precisely the truncated version of U(1). Using this property, we can reduce the qubit requirement 50%, down to $(n_\ell + 2)Q$ qubits. (Note that we need to use the argument θ instead of $e^{i\theta}$ in this case, and a sum $\theta + \theta'$ instead of a product $e^{i\theta} \cdot e^{i\theta'}$. Note also that, to have interactions, we need to add matter fields. See Supplementary Materials S5C for details.)

Finally, let us note that the simplest version of the singlet-projection protocol, translated into the \mathbb{Z}_2 gauge theory, requires only $n_\ell + 1$ qubits; we do not need an ancilla state $|Z\rangle_2$ in this case. Let $b = 0, 1$ corresponds to link variable $e^{\pi i b} = \pm 1$. The Haar random distribution on \mathbb{Z}_2 is $\frac{|0\rangle + |1\rangle}{\sqrt{2}} = \hat{h}|0\rangle$, where \hat{h} is the Hadamard gate. Therefore, $|\mathcal{G}\rangle = \frac{|0\rangle_\xi + |1\rangle_\xi}{\sqrt{2}}$ can be prepared easily. For example, let us take the case of $n_\ell = 2$. Suppose

the initial configuration was $\sum_{b_1, b_2} c_{b_1, b_2} |b_1\rangle_1 |b_2\rangle_2$. Furthermore, suppose that two links share one lattice point and transform by the \mathbb{Z}_2 transformation as $|b_1\rangle_1 |b_2\rangle_2 \rightarrow |b_1 \oplus 1\rangle_1 |b_2 \oplus 1\rangle_2$. In this case, we can obtain the counterpart of $|Z^{(\xi)}\rangle$ (i.e., $|b \oplus \xi\rangle$) using a CNOT gate (CX gate) that uses $|\xi\rangle$ as a control qubit. Therefore, the singlet projection goes as follows:

- We tensor $|0\rangle_\xi$ to this state to obtain $\sum_{b_1, b_2} c_{b_1, b_2} |b_1\rangle_1 |b_2\rangle_2 |0\rangle_\xi$
- Act the Hadamard gate on $|0\rangle_\xi$ to obtain $\sum_{b_1, b_2} c_{b_1, b_2} |b_1\rangle_1 |b_2\rangle_2 \frac{|0\rangle_\xi + |1\rangle_\xi}{\sqrt{2}}$
- Act $\text{CX}_{\xi, 1}$ to obtain $\sum_{b_1, b_2} c_{b_1, b_2} |b_2\rangle_2 \frac{|b_1\rangle_1 |0\rangle_\xi + |b_1 \oplus 1\rangle_1 |1\rangle_\xi}{\sqrt{2}}$
- Act $\text{CX}_{\xi, 2}$ to obtain $\sum_{b_1, b_2} c_{b_1, b_2} \frac{|b_1\rangle_1 |b_2\rangle_2 |0\rangle_\xi + |b_1 \oplus 1\rangle_1 |b_2 \oplus 1\rangle_2 |1\rangle_\xi}{\sqrt{2}}$
- Project to $|+\rangle_\xi$ to obtain $\sum_{b_1, b_2} c_{b_1, b_2} \frac{|b_1\rangle_1 |b_2\rangle_2 + |b_1 \oplus 1\rangle_1 |b_2 \oplus 1\rangle_2}{\sqrt{2}}$

As far as the time evolution is concerned, we can even use *harmonic oscillator* for a demonstration — if we apply the universal framework to the harmonic oscillator, what we get is the same universal kind of circuit [21]! The concrete circuit has been described already in ref. [50], though its fundamental importance has not been appreciated back then. A possible bottleneck is the precision of quantum Fourier transform at large values of Q , and harmonic oscillator is a perfect setup to study it comparing it with analytic results. More generally, one-boson system with a p -th order polynomial such as the double-well potential ($p = 4$). The gate requirement is $O(Q^p)$ for CNOT gates and one-qubit rotations, and $O(Q^2)$ for quantum Fourier transform.

[1] C.-N. Yang and R. L. Mills, Phys. Rev. **96**, 191 (1954).
[2] M. E. Peskin and D. V. Schroeder, *An Introduction to quantum field theory* (Addison-Wesley, Reading, USA, 1995).
[3] S. Weinberg, *The quantum theory of fields. Vol. 2: Modern applications* (Cambridge University Press, 2013).
[4] M. Y. Han and Y. Nambu, Phys. Rev. **139**, B1006 (1965).
[5] H. Fritzsch, M. Gell-Mann, and H. Leutwyler, Phys. Lett. B **47**, 365 (1973).
[6] D. J. Gross and F. Wilczek, Phys. Rev. Lett. **30**, 1343 (1973).
[7] H. D. Politzer, Phys. Rev. Lett. **30**, 1346 (1973).
[8] S. L. Glashow, Nucl. Phys. **22**, 579 (1961).
[9] S. Weinberg, Phys. Rev. Lett. **19**, 1264 (1967).
[10] A. Salam, Conf. Proc. C **680519**, 367 (1968).
[11] G. 't Hooft, Nucl. Phys. B **35**, 167 (1971).
[12] G. 't Hooft and M. J. G. Veltman, Nucl. Phys. B **44**, 189 (1972).
[13] J. M. Maldacena, Adv. Theor. Math. Phys. **2**, 231 (1998), arXiv:hep-th/9711200.
[14] S. N. Bose, Zeitschrift für Physik **26**, 178 (1924).
[15] A. Einstein, Sitzungsberichte der Preußischen Akademie der Wissenschaften, Physikalisch-Mathematische Klasse, 261 (1924).
[16] A. Einstein, Sitzungsberichte der Preußischen Akademie der Wissenschaften, Physikalisch-Mathematische Klasse, 3 (1925).
[17] R. P. Feynman, Phys. Rev. **91**, 1301 (1953).
[18] The origin of this widespread misconception is not clear. The claim that physical states must be gauge-invariant is often attributed to Kogut and Susskind [41], but their actual statement was “*The physical states are drawn from the space of gauge-invariant states*”, which describes a particular choice of basis convenient for their Hamiltonian lattice formulation. The physical content resides in gauge-equivalence classes; gauge-invariant represen-

tatives are one valid choice among many. In the past, non-singlet descriptions played crucial roles in the understanding of confinement in the large- N gauge theories [32] and emergent geometry in string theory [51, 52]. See also refs. [53, 54] that emphasized the difference between *physical* and *gauge-invariant*.

- [19] A. J. Buser, H. Gharibyan, M. Hanada, M. Honda, and J. Liu, JHEP **09**, 034, arXiv:2011.06576 [hep-th].
- [20] G. Bergner, M. Hanada, E. Rinaldi, and A. Schafer, JHEP **05**, 234, arXiv:2401.12045 [hep-th].
- [21] Halimeh, Jad C. and Hanada, Masanori and Matsuura, Shunji and Nori, Franco and Rinaldi, Enrico and Schäfer, Andreas, (2024), arXiv:2411.13161 [quant-ph].
- [22] G. Bergner and M. Hanada, (2025), arXiv:2506.00755 [quant-ph].
- [23] J. C. Halimeh, M. Hanada, and S. Matsuura, (2025), arXiv:2506.18966 [quant-ph].
- [24] M. Hanada, S. Matsuura, E. Mendicelli, and E. Rinaldi, (2025), arXiv:2505.02553 [quant-ph].
- [25] T. Kugo and I. Ojima, Prog. Theor. Phys. Suppl. **66**, 1 (1979).
- [26] A. M. Childs and N. Wiebe, Quant. Inf. Comput. **12**, 0901 (2012), arXiv:1202.5822 [quant-ph].
- [27] T. J. Yoder, G. H. Low, and I. L. Chuang, Phys. Rev. Lett. **113**, 210501 (2014), arXiv:1409.3305 [quant-ph].
- [28] A. Gilyén, Y. Su, G. H. Low, and N. Wiebe, in *51st Annual ACM SIGACT Symposium on Theory of Computing* (2018) arXiv:1806.01838 [quant-ph].
- [29] Note that wave packets cannot have a nontrivial stabilizer; any non-constant g moves all wave packets. With the standard boundary condition $g \rightarrow \mathbf{1}$, the stabilizer group can only be $\{\mathbf{1}\}$.
- [30] Sec. III discusses an implementation of this projection on digital quantum computer.
- [31] Note that typical values of $\|\hat{g} - \mathbf{1}\|$ increases with the number of lattice points (and also with $N^2 - 1$ in the case of $SU(N)$ theory), while only an $O(1)$ values is needed to suppress the overlap between $|\Phi\rangle$ and $\hat{g}|\Phi\rangle$.
- [32] M. Hanada, H. Shimada, and N. Wintergerst, JHEP **08**, 039, arXiv:2001.10459 [hep-th].
- [33] Refs. [55, 56] introduced a singlet-projection protocol for QCD in $1 + 1$ dimensions, utilizing a special property specific to $1 + 1$ dimensions to make the implementation tractable. We do not use any properties specific to certain dimensions, gauge group, or matter content. This makes our approach readily applicable to real-world QCD, and at the same, more resource-intensive.
- [34] If $|P=0\rangle$ exists in the truncated Hilbert space, we could introduce $|P=0\rangle_2$ and act $\exp\left(-i\text{Tr}\left(\hat{P}_2\hat{\bar{Z}}_1^{(\xi)} + \hat{P}_2\hat{Z}_1^{(\xi)}\right)\right)$ to get $|Z\rangle_1\left|Z^{(\xi)}\right\rangle_2|\xi\rangle$.

(In our specific truncation, exact zero-momentum mode does not exist, though it can be introduced slightly changing the details.) Then, by relabeling 1 and 2, the rest goes the same.

- [35] See Supplementary Material S4 for an alternative approach.
- [36] We can even take $g^2 \rightarrow 0$ at fixed lattice spacing a , which is a weaker coupling than the continuum limit. Such a trick can be useful when we use adiabatic state preparation.
- [37] J. R. Stryker, Phys. Rev. A **99**, 042301 (2019), arXiv:1812.01617 [quant-ph].
- [38] A. Rajput, A. Roggero, and N. Wiebe, npj Quantum Inf. **9**, 41 (2023), arXiv:2112.05186 [quant-ph].
- [39] M. Creutz, Phys. Rev. D **21**, 2308 (1980).
- [40] M. Hanada, J. Liu, E. Rinaldi, and M. Tezuka, Mach. Learn. Sci. Tech. **4**, 045021 (2023), arXiv:2212.08546 [quant-ph].
- [41] J. B. Kogut and L. Susskind, Phys. Rev. D **11**, 395 (1975).
- [42] E. Zohar, J. I. Cirac, and B. Reznik, Rept. Prog. Phys. **79**, 014401 (2016), arXiv:1503.02312 [quant-ph].
- [43] K. G. Wilson, Phys. Rev. D **10**, 2445 (1974).
- [44] L. Susskind, Phys. Rev. D **20**, 2610 (1979).
- [45] D. B. Kaplan, E. Katz, and M. Unsal, JHEP **05**, 037, arXiv:hep-lat/0206019.
- [46] M. Unsal, JHEP **11**, 013, arXiv:hep-lat/0504016.
- [47] T. Eguchi and H. Kawai, Phys. Rev. Lett. **48**, 1063 (1982).
- [48] P. Kovtun, M. Unsal, and L. G. Yaffe, JHEP **12**, 034, arXiv:hep-th/0311098.
- [49] E. Rinaldi, X. Han, M. Hassan, Y. Feng, F. Nori, M. McGuigan, and M. Hanada, PRX Quantum **3**, 010324 (2022), arXiv:2108.02942 [quant-ph].
- [50] N. Klco and M. J. Savage, Phys. Rev. A **99**, 052335 (2019), arXiv:1808.10378 [quant-ph].
- [51] M. Hanada, Phys. Rev. D **103**, 106007 (2021), arXiv:2102.08982 [hep-th].
- [52] V. Gautam, M. Hanada, and A. Jevicki, JHEP **01**, 019, arXiv:2406.13364 [hep-th].
- [53] V. Gautam, M. Hanada, A. Jevicki, and C. Peng, JHEP **01**, 003, arXiv:2204.06472 [hep-th].
- [54] J. R. Fliss, A. Frenkel, S. A. Hartnoll, and R. M. Soni, SciPost Phys. **18**, 171 (2025), arXiv:2408.05274 [hep-th].
- [55] A. T. Than *et al.*, Nature Commun. **16**, 10288 (2025), arXiv:2501.00579 [quant-ph].
- [56] A. Chakraborty, R. Lewis, and C. A. Muschik, Phys. Rev. Res. **7**, 043162 (2025), arXiv:2510.08718 [quant-ph].